2020

Developing Machine Learning Algorithms for Behavior Recognition from Deep Brain Signals

Hosein Golshan Mojdehi

Developing Machine Learning Algorithms for Behavior Recognition from Deep Brain Signals

_____

A Dissertation

Presented to

the Faculty of the Daniel Felix Ritchie School of Engineering and Computer Science

University of Denver

_____

In Partial Fulfillment

of the Requirements for the Degree

Doctor of Philosophy

_____

by

Hosein Golshan Mojdehi

August 2020

Advisors: Prof. Mohammad H. Mahoor and Dr. Adam O. Hebb

Author: Hosein Golshan Mojdehi
Title: Developing Machine Learning Algorithms for Behavior Recognition from Deep Brain Signals
Advisors: Prof. Mohammad H. Mahoor and Dr. Adam O. Hebb
Degree Date: August 2020

Abstract

Parkinson's disease (PD) is a neurodegenerative condition and movement disorder that appears with symptoms such as tremor, rigidity of muscles and slowness of movements. Deep brain stimulation (DBS) is an FDA-approved surgical therapy for essential tremor and PD. Despite the fact that DBS substantially alleviates the motor signs of PD, it can cause cognitive side effects and speech malfunction mainly due to the lack of adaptivity and optimality of the stimulation signal to the patients' current state. A behavior-adapted closed-loop DBS system may reduce the side effects and power consumption by adjusting the stimulation parameters to patients' need.

Behavior recognition based on physiological feedbacks plays a key role in designing the next generation of closed-loop DBS systems. Hence, this dissertation is concentrated on: 1. Investigating the capability of local field potential (LFP) signals recorded from Subthalamic nucleus (STN) in identifying behavioral activities 2. Developing advanced machine learning algorithms to recognize behavioral activities using LFP signals 3. Investigating the effects of medication and stimulation pulse on the behavior recognition task as well as characteristics of the LFP signal.

STN-LFP is a great physiological signal candidate since the stimulation device itself can record it, eliminating the need for additional sensors. Continuous wavelet transform is

utilized for time-frequency analysis of STN-LFPs. Experimental results demonstrate that different behaviors create different modulation patterns in STN within the beta frequency range.

A hierarchical classification structure is proposed to perform the behavior classification through a multi-level framework. The beta frequency components of STN-LFPs recorded from all contacts of DBS leads are combined through an MKL-based SVM classifier for behavior classification. Alternatively, the inter-hemispheric synchronization of the LFP signals measured by an FFT-based synchronization approach is utilized to pair up the LFP signals from left and right STNs. Using these rearranged LFP signals reduces the computational cost significantly while keeping the classification ability almost unchanged.

LFP-Net, a customized deep convolutional neural network (CNN) approach for behavior classification, is also proposed. CNNs learn different feature maps based on the beta power patterns associated with different behaviors. The features extracted by CNNs are passed through fully connected layers, and, then to the softmax layer for classification.

The effect of medication and stimulation “off/on” conditions on characteristics of LFP signals and the behavior classification performance is studied. The beta power of LFP signals under different stimulation and medication paradigms is investigated. Experimental results confirm that the beta power is suppressed significantly when the patients take medication or therapeutic stimulation. The results also show that the behavior classification performance is not impacted by different medication or stimulation conditions.

Identifying human behavioral activities from physiological signals is a stepping-stone toward adaptive closed-loop DBS systems. To design such systems, however, there are

other open questions that need to be addressed, which are beyond the scope of this dissertation, such as developing event-related biomarkers, customizing the parameter of DBS system based on the patients' current state, investigating the power consumption and computational complexity of the behavior recognition algorithms.

Acknowledgements

It is a great pleasure to express my deepest gratitude to my advisors, Prof. Mohammad H. Mahoor and Dr. Adam O. Hebb for their support, guidance and encouragement in this fascinating field. They motivated me to pursue novel ideas and provided me with exceptional experience and knowledge. I am forever grateful to them.

My special thanks go to Dr. Sara Hanrahan and Joshua Nedrud for their significant contributions in data recording sessions and their constant support for data analysis.

I would like to express my sincere appreciations to my committee members, Prof. Bradley Davidson, Prof. Mohammad Matin, and Prof. Daniel Linseman for their invaluable comments in improving this dissertation. I truly appreciate their time and consideration.

I am very thankful to all my friends and colleagues at the University of Denver and Computer Vision Lab, especially Sina Parhizi, Rohola Zandie, and Dr. Pooran Negi.

I would like to express my sincerest gratitude and love to my parents and brother, without their boundless support, encouragement, and sacrifice this would not be possible. I must express my most special appreciations to my lovely wife who has been my constant source of support and encouragement throughout this journey. I feel blessed to have such an amazing family and I am truly thankful to them.

I would like to thank Medtronic Inc for providing us with data recording equipment and their invaluable technical supports, especially Scott Stanslaski.

Last but not least, this research was partially supported by a grant from Knobel Institute for the Longevity and Health at the University of Denver and I thank them for their support.

Table of Contents

List of Figures

List of Tables

List of Abbreviations

FDA	Food and Drug Administration
PD	Parkinson's Disease
LFP	Local Field Potential
EEG	Electroencephalography
ECoG	Electrocardiography
EMG	Electromyography
ECG	Electrocardiography
ERP	Event-Related Potential
ERD	Event-Related Desynchronization
INS	Implantable Neuro-Stimulator
MRI	Magnetic Resonance Imaging
CT	Computed Tomography
IPG	Implantable Pulse Generator
IRB	Institutional Review Board
GPi	Internal Globus Pallidum
DBS	Deep Brain Stimulation
BCI	Brain Computer Interface
CSP	Common Spatial Pattern
STN	Subthalamic Nucleus
MI	Motor Imaginary
VIM	Ventral Intermediate
CNN	Convolutional Neural Network
SVM	Support Vector Machine
MKL	Multiple Kernel Learning
DNN	Deep Neural Network
DBN	Deep Belief Network
SAE	Stacked Auto-Encoders
HMM	Hidden Markov Model
FFT	Fast Fourier Transform
RBF	Radial Basis Function
PLV	Phase Locking Value
LOOCV	Leave-One-Out Cross Validation
ANN	Artificial Neural Network
ReLU	Rectified Linear Unit
PCA	Principal Component Analysis
PSD	Power Spectrum Density
KNN	K-Nearest Neighborhood

CHAPTER 1

INTRODUCTION

1.1 Parkinson's Disease

Parkinson's disease (PD) is a neurodegenerative disorder that appears with movement signs such as tremor, rigidity, and bradykinesia. The signs of PD are usually augmented by speech and alternate limb motor tasks [1]. The prevalence of PD increases with aging. Although the neurophysiological basis for this disease is not fully elucidated, loss of the neurotransmitter dopamine, a key regulator of basal ganglia function, leads to a dysfunctional interaction between the cortex and basal ganglia. The loss of dopamine in the striatum results in pathological connectivity between members of the basal ganglia leading to augmented beta frequency (10–30 Hz) oscillatory power in the local field potential (LFP) [2].

Primary motor signs of Parkinson's disease include the following, although not all symptoms appear in one patient:

- Tremor of the hands, arms, legs, jaw and face
- Bradykinesia or slowness of movement
- Rigidity of the limbs and trunk
- Postural instability or impaired balance and coordination

1.2 Deep Brain Stimulation

Deep brain stimulation (DBS) therapy for PD consists of implanting passive electrical leads into regions of the basal ganglia such as the Globus Pallidum (GPi) or Subthalamic Nuclei (STN). A neuro-stimulation pulse generator capable of generating high-frequency (~130-185 Hz) electrical stimulation is implanted subcutaneously to supply the DBS leads with therapeutic stimulation [3,4]. Apart from providing relief of the PD symptom manifestations, DBS gives a unique opportunity to record in vivo the neural activities in deep brain structures through recording local field potential (LFP) signals in surgery [1]. This provides an excellent opportunity to investigate the electrical oscillatory activities of the brain [5,6].

Prior to the surgery, magnetic resonance imaging (MRI) or computed tomography (CT) scanning is performed on the patient to identify and pinpoint the exact target within the brain for surgical implantation [7,8]. The possibility of bleeding or infection during the placement of the stimulator is very low.

Microelectrode recording is sometimes used to monitor the activity of nerve cells in the target area more precisely [9]. In general, the most common target areas of the brain include thalamus, subthalamic nucleus, and globus pallidus.

As shown in figure 1.1, the DBS system consists of three components: the lead, the extension, and the IPG (implantable pulse generator). The lead is an insulated slim rod inserted through a small opening in the skull. The extension is an insulated wire, which goes under the skin of the head, neck, and shoulder to connect the lead to the IPG. The IPG is usually implanted subcutaneously, which generates the electrical pulse to stimulate

specific regions in the brain. In some cases it may be implanted lower in the chest or under the skin over the abdomen. The electrical pulses are generated by the IPG and sent via extension wire and the lead into the target area in the brain. These therapeutic pulses are able to bypass abnormal electrical signals and mitigate PD motor symptoms.

Generally, DBS uses electrical stimulation to regulate electrical signals in neural circuits in the brain to improve PD symptoms. Since the DBS surgery does not make dramatic permanent changes in the brain structure, if DBS causes unwanted side effects, the implantable pulse generator can be removed, and the DBS procedure can be halted which is remarkable advantage of the DBS treatment. In addition, the IPG parameters and the characteristics of the stimulation pulse are adjustable without further surgery if the persons condition changes. New generation of DBS devices (Activa^{TM} PC+S) can be programmed through a radio device in a completely non-invasive procedure.

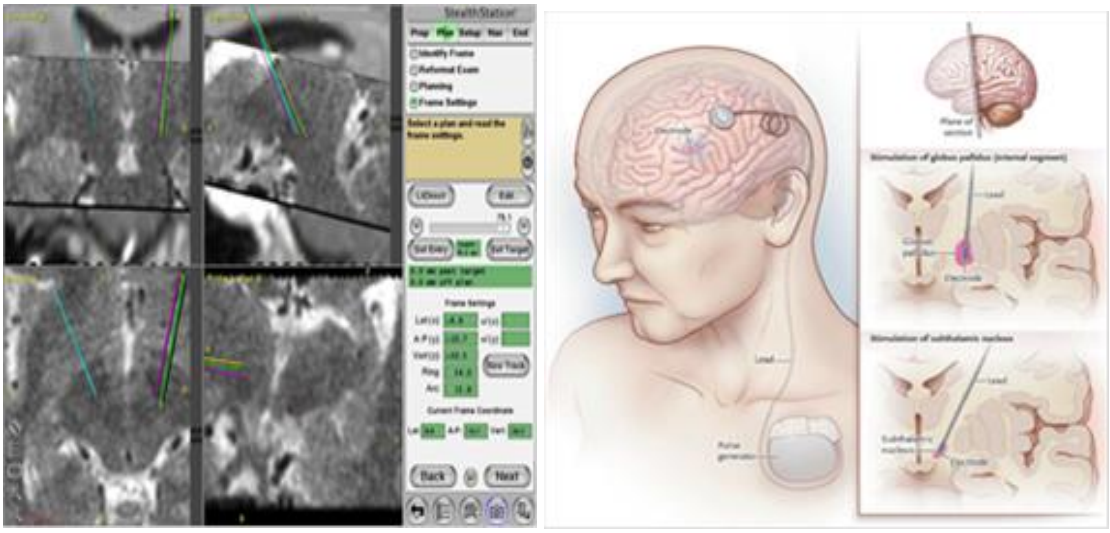

Figure 1.1. A typical DBS system and brain MRI scans for DBS lead implantation. Left shows the MRI scan of the brain and the trajectory of DBS lead implantation on the workstation before surgery. Right shows a typical implanted DBS system [Medtronic Inc].

The DBS surgery is very effective in reducing the patients' motor symptoms; however, most patients still need to take some levels of medication after the surgery. The dosage of medication varies depending on the patient's condition, but can be considerably reduced in most patients. DBS does not improve cognitive symptoms in PD and indeed may worsen them, so it is not generally used if there are signs of dementia [10].

1.3 Behavior Recognition through Brain Signals

Deep brain stimulation (DBS) therapy for PD consists of implanting passive electrical leads into regions of the basal ganglia such as the Globus Pallidum (GPi) or Subthalamic Nuclei (STN). A neuro-stimulation pulse generator capable of generating high-frequency (~130-185 Hz) electrical stimulation is implanted subcutaneously to supply the DBS leads with therapeutic stimulation [3,4] (Figure 1.2).

DBS provides a unique opportunity to record *in vivo* the neural responses through acquiring LFP signals [1], allowing the investigation of electrical oscillatory activities of the brain [6,11]. Apart from characterizing the neural activity within cortical regions and subcortical nuclei [2], human LFP recordings have been used to study the effect of neuro-stimulation as well as designing primitive closed-loop DBS systems [12-14]. Specifically, LFPs recorded from the STN have shown to be robust control signals indicating a change in the patients' state [15,16], correlating with the patients' PD symptoms, medication level, and behavior [1,17,18]. LFP signals are stable over long periods of time [5,19], which is a necessary characteristic for a feedback signal in a closed-loop DBS system.

Recognition of human behavior through neural feedbacks from the brain is a stepping-stone for designing a closed-loop DBS system that can adaptively change the parameters

of the stimulation signals. To this end, electroencephalography (EEG) and LFP signals have been used to decode human behavior. Note that an accurate behavior classification based on the brain signals is challenging due to poor signal-to-noise ratio [20,21].

So far, various EEG-based classification and detection algorithms have been developed [22-24]. Event-related potential (ERP)-based classification has been used for designing brain computer interfaces (BCI) [25,26]. Several approaches have been proposed for EEG classification using support vector machines (SVM) [27,28]. Common spatial pattern (CSP) has been one of the most popular approaches for single-trial EEG classification [29-31]. Many studies have focused on the real-time detection of behavior using EEG and electrocorticography (ECoG) data such as P300 detection for spelling [32,33], brain-switch based on motor imagery [34], and self-regulation of rhythm [23]. Most recently, deep neural networks (DNN) have gained considerable attention for numerous classification and regression tasks. A deep belief network (DBN) model was proposed by [35] for binary motor imaginary (MI) classification and obtained better performance compared to SVM. DBN has also been used in other related studies for anomaly measurement of EEG signals [36]. Convolutional neural network (CNN) was used to classify MI using EEG signals [37]. CNN and stacked auto-encoders (SAE) was used to classify EEG MI signals [38].

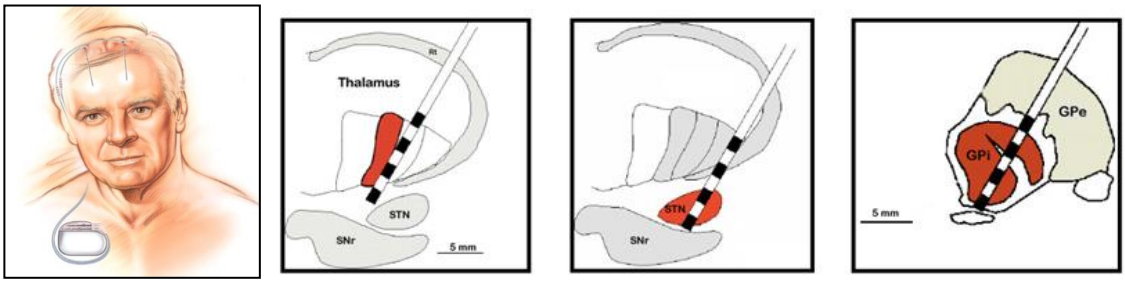

Figure 1.2. DBS targets in the brain. left shows a typical implanted DBS system and right shows three

Human behavior classification using STN-LFPs has been studied in the related literature. Loukas and Brown [18] proposed an algorithm to predict self-paced hand movements based on the oscillatory nature of the STN-LFPs. Santaniello et al. [13] designed a primitive closed-loop DBS system capable of adjusting the stimulation amplitude. The LFP signals from the ventral intermediate nucleus (VIM) of the thalamus were used as the control variable in their closed-loop system. Time-frequency analysis of the beta frequency range (f~10–30 Hz) of LFP signals has been used in different studies [39-43] to drive SVM or multiple kernel learning (MKL)-based SVM classifiers for human behavior recognition purposes. A hybrid model based on combining SVM and hidden Markov model (HMM) was proposed in [44] for human behavior classification. In [45] a non-linear regression method was developed to measure the inter-hemispheric connectivity between LFP signals, aiming at detecting the motor activity of PD patients.

1.4 Basal Ganglia Modulation with Behavioral Activity

Analyzing the connectivity of different brain structures and circuitry (Figure 1.3) has gain considerable attention in the recent years. As shown in figure 1.3, basal ganglia receives information from cerebral cortex, and the outputs return to the frontal cortex or the motor systems in the midbrain and the hindbrain. Various areas of cerebral cortex are connected to regions of striatum and via pallidus and thalamus return back to the frontal cortex. There is a less direct pathway from the striatum via the external pallidus and STN, and there is a shorter route from thalamus to striatum that bypasses the cerebral cortex.

Among various signals that can be collected from the brain, we focused on the local field potentials (LFP) recorded from the STN, as it has been shown that it is a reliable candidate for human behavioral analysis as well as the PD conditions over time [1,2]. Moreover, STN-LFP is a suitable choice for a closed-loop DBS system since it can be recorded and processed without need for any additional sensors attached to the patients. LFP is the electric potential recorded in the extracellular space in brain tissue, typically using micro-electrodes. Not that, LFPs are different from the electroencephalogram (EEG), which is recorded at the surface of the scalp using macro-electrodes. It also differs from the electro-corticogram (ECoG), which are recorded from the surface of the brain using

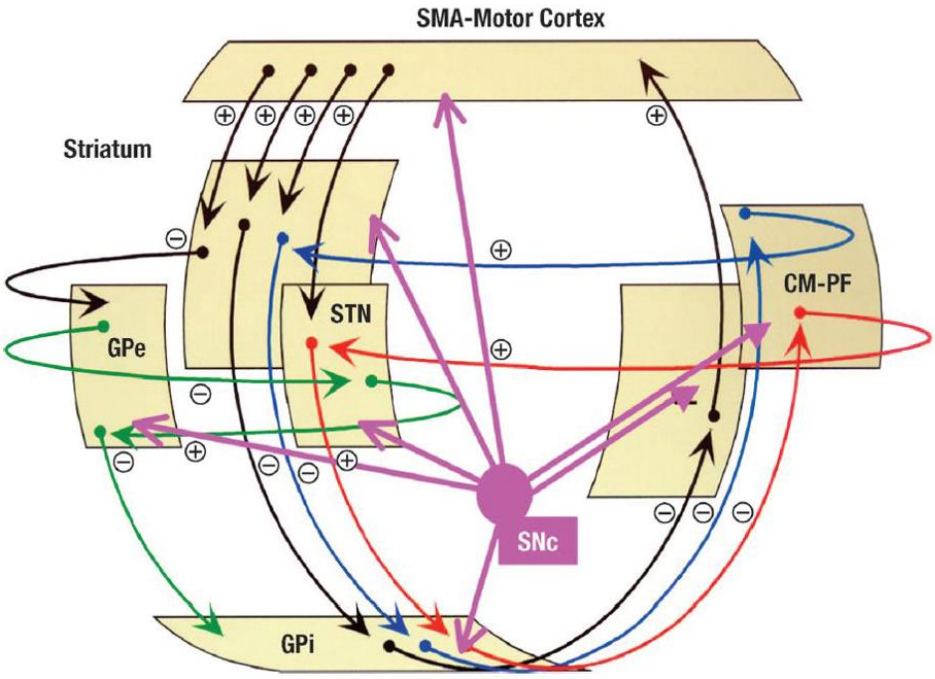

Figure 1.3. A typical map of the basal ganglia network and interaction between different brain structures inside the basal ganglia. SMA: supplementary motor area; GPe: external globus palidus; STN: subthalamic nucleus; CM-PF: centre median-parafascicular; SNc: substantia nigra pars compacta; GPi: internal globus pallidus. + and – signs respectively indicates the excitatory and inhibitory effects [46].

large subdural electrodes. On the other hand LFPs are recorded in depth of the cortical tissue or other deep brain structures (see figure 1.4 for details).

It has been shown that the rhythm of Basal ganglia network inside the brain is modulated by behavioral activities, which appear by changing the power of oscillations [1,2]. Moreover, the time-frequency analysis of STN-LFP signals shows that the beta frequency spectral power is suppressed during behavioral tasks, leading to beta oscillations gets desynchronized with activity as opposed to its relatively synchronized behavior during rest state [1,2]. The continuous spectrum of the brain signals are usually analyzed based on several bandwidths, including delta (0.5-3)Hz, theta (3-8)Hz, alpha (8-12)Hz, beta (12-32)Hz, and gamma (32-100)Hz. Each of these frequency bands corresponds to a specific condition. Brainwaves change based on the subject's current status; slower brainwaves are related to tiredness, slowness, sluggishness, or dream. On the other hand, higher frequencies are dominant during hyper-alert situations. A typical spectrum of various

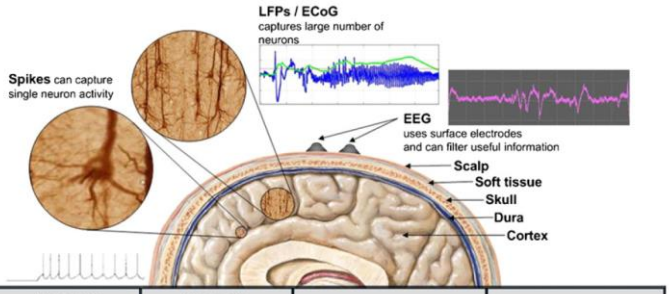

Sensing Methodology	Chronic Recording	Information Coding	System Power
Spike Recording	Challenging Interface Stability	High Fidelity, Need Ensemble Averages for Disease State	High Bandwidth/ Power & Data Processing Req.
Field Potentials	Less Sensitive to Interface Stability, Reuse Existing Technology	Medium Fidelity, Direct Relation to Disease State	Less Bandwidth/ Power & Data Processing Req.
Surface EEG	Irritation High Interference	Lower Fidelity, Less Spatial, Temporal, & Spectral Resolution	External Power Source Can Be Used

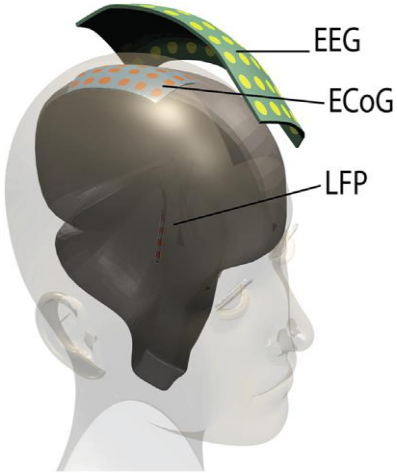

Figure 1.4. Recording different brain signals. left shows a comparison between different recording setups. Right shows the normal recording locations of EEG, ECoG and LFP signals [47].

bandwidth of the brainwave is shown in figure 1.5. Moreover, more details on the different bandwidth are given in the followings [48,49]:

- **Delta bandwidth (0.5-3)Hz:** Delta-band brainwave is the slowest and loudest brainwave. It is generated in deepest meditation and dreamless sleep. Delta waves suspend external awareness and are the source of empathy. Healing and regeneration are stimulated in this state, and that is why deep restorative sleep is so essential to the healing process.
- **Theta bandwidth (3-8)Hz:** Theta-band brainwave most often occurs during sleep and are also dominant during the deep meditation. It acts as our gateway to learning and memory. Theta waves coincides with dream, imagination, intuition, and information beyond our normal conscious awareness. It is where we hold our fears, troubled history, and nightmares.

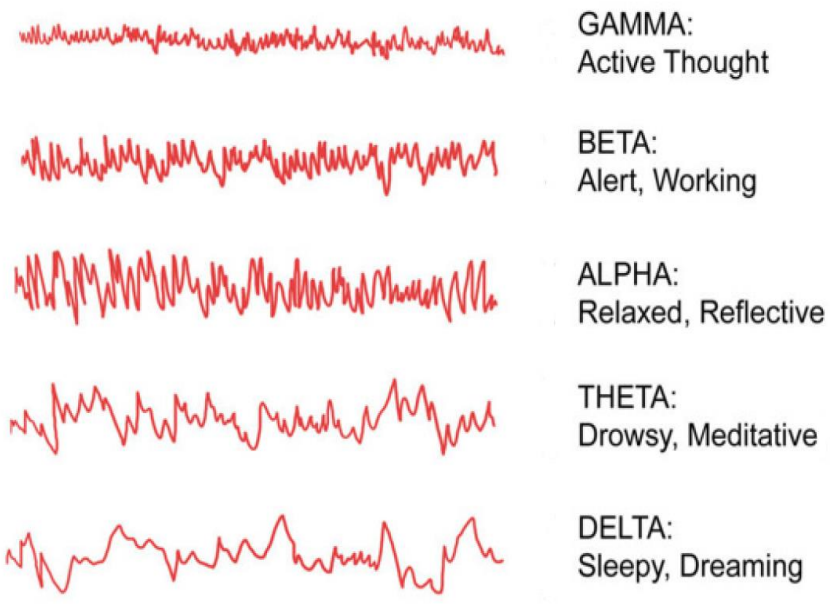

Figure 1.5. A typical spectrum of various bandwidth of the brainwave [48]

- **Alpha bandwidth (8-12)Hz:** Alpha-band brainwave is dominant during quiet thoughts as well as some meditative states. Alpha is the resting state for the brain. Alpha wave assists with mental coordination, calmness, alertness, mind/body integration and learning.
- **Beta bandwidth (12-32)Hz:** Beta-band brainwave dominates the normal state of consciousness when attention is directed towards cognitive tasks and the outside world. Beta is a fast activity, when we are alert, attentive, engaged in problem solving, decision making, and engaged in focused mental activity.
- **Gamma bandwidth (32-100)Hz:** Gamma-band contains the highest frequency brainwaves and relates to simultaneous processing of information from different brain areas. It passes information rapidly. Gamma was traditionally dismissed as "spare brain noise" until it was discovered that it is highly active during states of love, altruism, and the higher virtues. Gamma rhythms modulate perception and consciousness, and disappears under anesthesia. Gamma is also above the frequency of neuronal firing, so how it is generated remains a mystery.

1.5 Goals, Impacts, and Contributions

DBS alleviates the motor symptoms of PD but may lead to side effects such as impaired cognition, speech, gait, and balance [50-53]. DBS therapeutic stimulation is optimized in a controlled medical environment, and typically only a single set of static parameters are programmed. Over-optimizing DBS therapy for one behavior (e.g., walking) may come at a cost such as side effects for another behavior (e.g., talking). An adaptive closed-loop DBS

system (Figure 1.6) could provide unique parameters for disparate behavior, providing superior therapeutic benefit for the task at the moment, without the cost of compromising performance for tasks performed later [54-58]. Therefore, a closed-loop DBS system can decrease the side effects (e.g., cognitive and balance disruptions) of the existing open-loop DBS systems, which only use constant stimulation parameters such as frequency, pulse width, and amplitude.

Additionally, a closed-loop system may reduce the power consumption of DBS systems by switching off/on the implanted pulse generator when needed [12]. Currently, the stimulation parameters are set by highly trained clinicians, and the initial programming may require multiple clinical visits over several months before achieving optimal performance. Over the lifetime of the device, the stimulation parameters may need to be adjusted periodically in order to obtain a suitable compromise between maximization of the therapeutic improvement and minimization of the stimulation-imposed side effects [57,59]. The static nature of current FDA-approved DBS devices are poorly consistent with

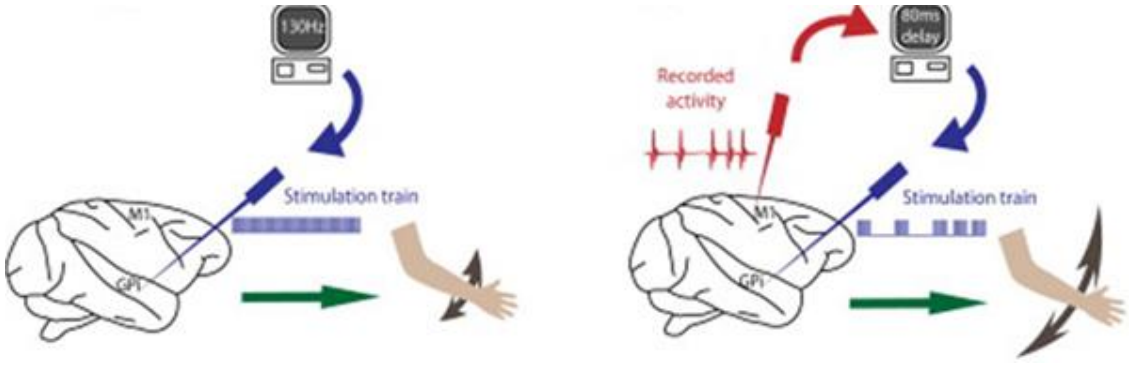

Figure 1.6. Left and right figures respectively show a typical open-loop and closed-loop DBS system [13].

the dynamic nature of PD since the Parkinsonian symptoms have typically faster dynamics than those provided by the adjustments of the DBS therapy [57,58].

Hence, developing a closed-loop DBS system capable of adjusting the stimulation parameters automatically is of high importance. To this end, recognition of the human behavior using the feedback of electrical signals recorded from brain is considered a major stepping stone toward such a device. This fact motivated us to take steps toward this dissertation. The main objective of our research is to analyze the capabilities of brain signals as bio-feedbacks for recognition of human behavior, which plays an important role in designing the next generation of adaptive closed-loop systems. Note that behavioral level closed-loop DBS system is advantageous due to the fact that for some specific behaviors such as "speech" the stimulation can be problematic, and, therefore, behavior recognition is essential in developing an efficient closed-loop system.

The main goals of this dissertation revolve around the following objectives:

- Developing a reliable feature space using the local field potential (LFP) signal recorded from the brain subthalamic region, based on which different behavioral activities can be recognized.
- Developing an efficient classification algorithm to decode the recorded LFP and classify the behavior associated with it.
- Investigating the effects of medication and stimulation pulse on the characteristics of the LFP signals as well as its impact on the behavior recognition algorithms.

To address the aforementioned problems, the main contributions are as follows:

- Time-frequency analysis of the LFP signals is investigated using continuous wavelet transform to design a feature space based on which the behavior recognition can be done properly.
- A hierarchical classification structure is developed to perform the behavior classification using LFP signals through a multi-level framework.
- A multiple kernel learning method is used to combine all bipolar signals recorded from two implanted DBS leads inside left and right STNs for each behavioral task. An FFT-based synchronization method is developed to evaluate the connectivity of the recorded LFPs from both STNs and its impact on the behavior classification task.
- An automated machine learning framework (LFP-Net) using deep convolutional neural networks is developed for classification of human behavior using the time-frequency representation of STN-LFPs. LFP-Net learns different feature maps based on the beta power patterns associated with different behaviors, leading to higher classification ability.
- A separate study is conducted on the effect of medication “off/on” and stimulation “off/on” conditions on characteristics of LFP signals as well as the behavior classification performance. STN-LFP signals of PD subjects are recorded chronically 12-24 months after DBS surgery and used in this study. The beta power suppression in LFP signals under different

stimulation/medication paradigms is investigated. The behavior classification performance is investigated in the presence of stimulation pulse.

The remainder of this dissertation is organized as follows: chapter 2 presents the STN-LFP data recording procedure. Moreover, the feature extraction method used in this dissertation will be presented in this chapter. A review of the analytical methods used for behavior classification will also be given in chapter 2. Chapter 3 elaborates on the proposed hierarchical classification approach for behavior classification. Chapter 4 presents the LFP-Net, the deep learning framework proposed for behavior classification using STN-LFP signals. Chapter 5 discusses the effect of medication and stimulation pulse on the behavior classification performance. Finally, chapter 6 concludes this dissertation and presents some of the possible future work and research roadmap.

CHAPTER 2

DATA RECORDING and ANALYSIS METHODS

2.1 Materials and Data Recording Details

Three separate datasets were collected during standard of care DBS surgery for treatment of idiopathic PD. Two datasets were collected at the Colorado Neurological Institute (Denver, CO, USA) and the other dataset was collected at the University of Washington (Seattle, WA, USA). All participants provided informed consent in a manner approved by their respective Institutional Review Boards (IRB). The recording sessions were carried out on each subject using DBS leads (Medtronic 3389, Minneapolis, MN, USA) bilaterally implanted in the STN. The DBS lead electrode is a linearly ordered set of 4 platinum/iridium contacts (numbered from ventral/deep #0 to most dorsal/superficial #3). Each contact has a surface area of 6.0 mm^2 and an impedance of 1.7 kΩ (mean; 95% CI = 1.1–2.4 kΩ). Channels were bipolar re-referenced within each brain hemisphere (0–1, 1–2, 2–3) prior to analysis. A typical Medtronic DBS lead with four contacts as well as a coronal view of the DBS implantation in both STNs is shown in figure 2.1.

Dataset1 includes two PD subjects recruited for research purposes. In a separate surgery, an implantable neuro-stimulator (INS) with additional voltage recording capabilities was implanted subcutaneously to provide both standard therapeutic stimulation and bilateral local field potential (LFP) recordings [60]. For Dataset1, several postoperative INS recordings were chronically performed at 12 and 24 months after DBS lead implantation surgery under different medication off/on and stimulation off/on conditions (the medication "on" and stimulation "on" cases are separately studied in chapter 5). Two different behavioral tasks were designed for Dataset1, including 60 repetitions of cued "button press" and "target-reaching" trials performed by left or right hands in each recording session (see more details in Table 2.1). The "button press" task consisted of pressing a button using either the left or right thumb. The "target-reaching" task required the patients to raise their arm to reach a target appearing on the screen in front of their face

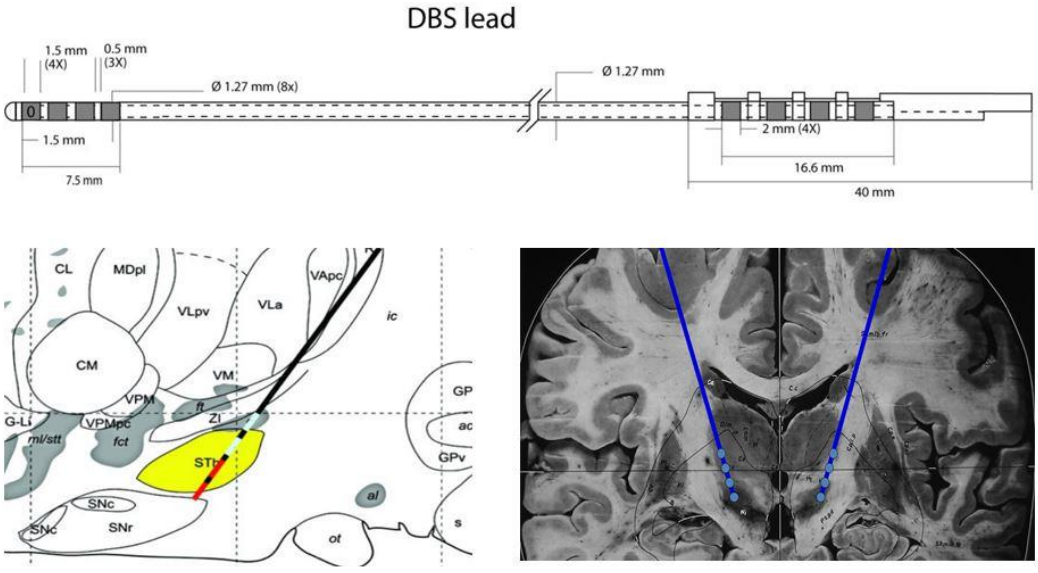

Figure 2.1. DBS leads implantation. Top shows a typical DBS lead with four contacts. Bottom left shows an atlas representation of the implanted DBS lead. Bottom right shows a coronal scan of the brain including two implanted DBS leads inside each STN [2].

Table 2.1. Dataset and recording details. Dataset1 includes several chronical recording sessions, so the number of trials is the summation of all sessions. Dataset2 and Dataset3 include only one recording session per subject. BP, TR, SP, and MM respectively stand for button press, target reaching, speech, and mouth movement behavioral activities

Dataset	Subject	Fs(Hz)	# recording channels (bipolar)	bandwidth(Hz)	#BP	#TR	#SP	#MM
Dataset1	1	422	2	0.5-100	120	120	0	0
	2	422	2	0.5-100	240	239	0	0
Dataset2	3	4800	6	1-1000	79	65	43	46
	4	4800	6	1-1000	90	88	45	43
	5	4800	6	1-1000	86	83	45	45
	6	4800	6	1-1000	89	84	45	45
Dataset3	7	5000	6	1-1000	30	0	54	0
	8	5000	6	1-1000	45	0	90	0
	9	5000	6	1-1000	45	0	71	0
	10	5000	6	1-1000	30	0	57	0

using either the left or right hand. Moreover, for Dataset1, only one bipolar re-referenced channel from each hemisphere was selected for recording and analysis (i.e., the channels that contained the most prominent peak in beta frequency oscillations were selected for further behavioral recordings).

Dataset2 and 3 include eight PD subjects in total (four subjects each) for whom the data recording was performed during the DBS implantation surgery. All subjects underwent bilateral recordings and all four contacts of each DBS lead were used for collecting signals. The recorded signals were bipolar re-referenced for post-processing purposes. All patients were in the off-medication and off-stimulation state and the recordings did not proceed until patients were fully awake during the surgery. Four different behavioral tasks were designed for Dataset2, including cued “button press”, “target-reaching”, “mouth movement”, and “speech” tasks. Dataset3, however, comprises cued “button press” and “speech” tasks. The “button press” task for Datasets 2 and 3 was performed in the same manner as described for Dataset1. The “speech” task included reciting simple

names/phrases displayed on a screen located in front of the patients' face. The "mouth movement" task simply comprised moving the mouth without speech. The "target-reaching" task required the patients to raise their arm to reach a target appearing on the screen using either the left or right hand.

Dataset1 was recorded using an Activa PC+S amplifier (Activa^{TM} PC+S, Medtronic, Inc.,), Dataset2 was recorded using a g.USBamp (g.tec, Graz, Austria) amplifier and Dataset3 was recorded using a Synamps2 (Neuroscan, Victoria, Australia) amplifier.

2.2 Time-Frequency Analysis of STN-LFP Signals

In this dissertation, the time-frequency representation of the recorded LFP signals is used to generate the feature space for the behavior classification methods. Note that, the time-frequency analysis of various brain signals (e.g., LFP and EEG) has been studied in some related literature [1,61]. It has been shown that the time-frequency domain is a better feature space to distinguish different human behaviors in comparison with raw signals recorded from the brain. Therefore, it can intrinsically improve the classification ability due to the more distinctive feature space. As shown in figure 2.2, here, for a LFP epoch sample $X(c,t)$ at bipolar contact c and time t, the third-order tensor $X(c,f,t)$ at bipolar contact c, frequency f, and time t is obtained by calculating the amplitude of the wavelet transform as follows:

$$X(c, f, t) = \left\| X(c,t) * \frac{1}{\sqrt{a}} \psi\left(\frac{t}{a}\right) \right\|. \tag{2.1}$$

The complex Morlet mother wavelet $\Psi(\mathrm{t}) = (1/\sqrt{\pi \mathrm{f_b}}) exp(-\mathrm{t}^2/\mathrm{f_b}) exp(\mathrm{j}2\pi \mathrm{f_c t})$ (f_c is the wavelet center frequency and f_b is the bandwidth parameter) has extensively been used

for biomedical signal processing applications including temporal analysis of the LFP signals [61,62]; hence, it is employed as the mother wavelet in this work as well. As we are interested in the β frequency band, the scaling variable 'a' of the wavelet function is set so as to obtain the frequency range f ~ 10-30 Hz (i.e., for the sampling frequency Fs, we have $a = \mathrm{F_s}/(\mathrm{f}/2)$).

Once the feature vectors are obtained, it is common to apply different dimensionality reduction approaches to reduce the size of feature vectors. As a result, the computational burden of other post-processing data analysis methods decreases considerably. In addition, it helps tackle the problem of the curse of dimensionality that may occur in high-dimensional data spaces. Hence, Principal Component Analysis (PCA) is utilized for

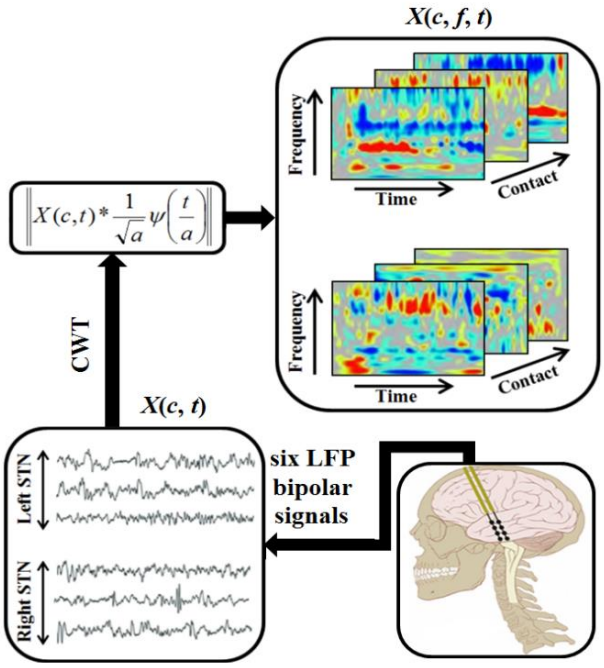

Figure 2.2. Wavelet-based feature extraction. From three left and three right bipolar LFP signals, the corresponding time-frequency components within the β frequency range are calculated using the complex Morlet mother wavelet. These wavelet coefficients are then used as features for human behavior classification.

dimensionality reduction purposes [63]. Essentially, PCA projects a set of N zero-mean input data $\mathrm{D} = \{\mathrm{x}_i \in R^d\}_{i=1}^N$ onto a set $\mathrm{D}' = \{\mathrm{x}_i \in R^k\}_{i=1}^N$, where $k \ll d$ is the set of linearly uncorrelated variables called principal components. These principal components correspond to the leading eigenvectors of the covariance matrix of D, and span a subspace that retains the maximum variance of the data.

2.3 MKL-based SVM Classifier

In chapter 3, a recently proposed Lp-norm MKL-based SVM classifier [64,65] is employed to design a hierarchical behavior classification method. MKL-based SVM classifier has successfully been applied on the STN-LFP signals for human behavior recognition purposes [40,41] and led to promising results specifically for combining multiple feature vectors. Hence, the main properties of the MKL-based SVM classifier are presented here.

In canonical SVM, the parameters of the kernel functions are usually tuned during the training phase, and the parameters that lead to the best classification accuracy on the validation set are used to classify the test sample. Since different kernels with different parameters correspond to different representations of the features, the MKL-based SVM classifier employs a combination of various kernel functions to automatically pick the optimal parameters. Several realizations of the MKL algorithm have already been presented in the literature [64-68]. However, in this study, a recently proposed Lp-norm MKL multiclass-SVM [65] is used, which considers both sparse and non-sparse kernel combinations within MKL formulation. As a consequence, it provides more flexibility in selecting different kernel combinations. The MKL-based SVM classifier learns both the

decision boundaries between different classes and kernel combination weights in a single optimization problem, improving the discriminant power of the SVM [66,67]. The formulation of the generalized Lp-norm MKL optimization problem for binary classification case is given as follows:

$$\begin{aligned} \min_{\boldsymbol{\omega},\omega_0,\boldsymbol{\xi}} \; & \mathrm{J}(\boldsymbol{\omega},\omega_0,\boldsymbol{\xi}) = \frac{1}{2}\|\boldsymbol{\omega}\|_{2,p}^2 + C\sum_{i=1}^{N}\boldsymbol{\xi}_i . \\ \text{s.t.} \; & y_i\left(\sum_{m=1}^{M}\boldsymbol{\omega}_m^T\varphi_m(\mathbf{x}_i)+\omega_0\right)\geq 1-\boldsymbol{\xi}_i , \\ & \boldsymbol{\xi}_{\mathrm{i}} \geq 0, \quad p\geq 1, \quad i = 1, 2, \ldots N \end{aligned} \tag{2.2}$$

where, $\varphi_m(\cdot)$ maps the feature vector x_i to another space based on which the kernel function $k(\cdot\,,\cdot) = \langle\varphi_m(\cdot),\varphi_m(\cdot)\rangle$ is defined. $\{\omega_{\mathrm{m}}\}$s are the parameters of the decision hyper-planes. M and N are the number of kernels and training samples respectively. C is the penalty parameter and ξ_i is the vector of slack variables. The parameter p in Eq. (2.2) is to regularize over kernel combination coefficients, which considers both sparse and non-sparse kernel combinations within MKL. Finally, y_i is the corresponding label of the training sample x_i. This convex optimization problem is solved using its dual form as follows:

$$\begin{aligned} & \min_{d}\max_{\alpha} \; L(d,\alpha) = \mathbf{1}^{\mathbf{T}}\boldsymbol{\alpha} - \frac{1}{2}\boldsymbol{\alpha}^{\mathbf{T}}\mathbf{Y}\mathbf{K_d}\mathbf{Y}\boldsymbol{\alpha} \qquad p\in[1,\,2). \\ & \max_{d}\max_{\alpha} \; L(d,\alpha) = \mathbf{1}^{\mathbf{T}}\boldsymbol{\alpha} - \frac{1}{2}\boldsymbol{\alpha}^{\mathbf{T}}\mathbf{Y}\mathbf{K_d}\mathbf{Y}\boldsymbol{\alpha} \qquad p\in(2,\,+\infty) \\ & s.t. \qquad \mathbf{K}_d = \sum_{m=1}^{M}\mathbf{d}_m\mathbf{K}^{(m)}, \quad \sum_{i=1}^{N}\boldsymbol{\alpha}_i y_i = 0, \\ & \qquad 0\leq\boldsymbol{\alpha}_i\leq C, \quad \sum_{m=1}^{M}\mathbf{d}_m^{p/(2-p)}\leq 1, \; \mathbf{d}_m\geq 0 \end{aligned} \tag{2.3}$$

where, $\mathrm{d} = (d_1, d_2, \ldots, d_{\mathrm{M}})^{\mathrm{T}}$ is the kernel combination vector that controls the weight of $(\|\omega\|^2)$ in the objective function of Eq. (2.2). $\alpha = (\alpha_1, \alpha_2, \ldots, \alpha_{\mathrm{N}})^{\mathrm{T}}$ is the vector of Lagrangian

dual variables corresponding to each training sample. Y = $diag(y_1, y_2, \ldots, y_N)$ is an $N \times N$ diagonal matrix, and $K^{(m)}$ is the kernel matrix corresponding to the m^{th} kernel function, $\mathbf{K}_{\mathbf{i,j}}^{(\mathbf{m})} = k(x_i, x_j)$. Consequently, the label y_z of each test sample $z \in R^D$ is obtained by:

$$y_z = \operatorname{sgn}\left(\sum_{i=1}^{N} \sum_{m=1}^{M} \boldsymbol{\alpha}_i y_i \mathbf{d}_m k_m(\mathbf{x}_i, \mathbf{z}) + \omega_0\right) \tag{2.4}$$

2.4 Deep Convolutional Neural Network

In chapter 4, LFP-Net, an automated machine learning framework based on deep convolutional neural networks (CNN) is presented and used for behavior classification using STN-LFP signals. So, an overview of the CNN architecture is presented here.

Deep convolutional neural networks have gained considerable attention in recent years with so many applications ranging from natural language processing to medical image analysis and image classification [69-71]. In contrast to the traditional artificial neural network (ANN), which is susceptible to shift and translation distortion, the CNN is both shift and translation invariant, making it more robust for classification of visual patterns. Essentially, CNNs are multi-layer neural networks composed of several convolution-pooling layers followed by nonlinearity activation units and fully connected layers. These layers are stacked such that the input data is passed through all connected layers to drive the output of the network.

At the convolutional layer, the input data is convolved with trainable filters to generate the output feature map. At each given convolutional layer, the k^{th} feature map is obtained by applying the corresponding filter as follows:

$$h_i^k = f\left(W^k * X + b_k\right) \tag{2.5}$$

where X and W^k are respectively the input data and the weights of the k^{th} filter, b_k is the bias term, and $f(\cdot)$ is the nonlinear activation function.

The pooling layer reduces the dimension of the output of the convolutional layer, leading to a lower computational burden and preventing the overfitting problem [69]. For instance, the max-pooling operation, as one of the well-known pooling operation, selects the maximum value of a small neighborhood of each feature map. The fully connected layer is fed by the flattened feature map obtained from the convolutional layers. Typically, several fully connected layers are stacked after the convolutional layer, where all the neurons are connected. However, a portion of connections between different layers may randomly be dropped if a dropout procedure is applied after a layer of the network [69].

Similar to ANN, the weights and biases of the CNN are calculated using a back-propagation algorithm [72], where the labeled training set is exposed to the network and the error "E" between the desired output and the predicted output by the network is calculated. This optimization procedure is done using a gradient descent algorithm such that "E" becomes minimized iteratively [72]:

$$\Delta W^k = -\eta \frac{\partial E}{\partial W^k},\ \Delta b^k = -\eta \frac{\partial E}{\partial b^k} \tag{2.6}$$

where, η is the learning rate that controls how fast the network learns during the training phase. The learning rate is experimentally set for a specific dataset and network architecture to obtain the best performance.

2.5 Statistical Analysis Approaches

In the machine learning context, using a k-fold cross validation approach, a paired student's t-test is usually used to check if the difference in the mean accuracy between the two models is statistically significant, e.g. reject the null hypothesis that assumes the two samples have the same distribution. In the case of the k-fold cross-validation, however, a paired student's t-test is weakly recommended since the observations in each sample are not independent. As part of the k-fold cross-validation procedure, a given observation will be used in the training dataset (k-1) times, leading to a high type-I error. Therefore, to perform the statistical analysis, two other approaches are used in this dissertation.

First, a Wilcoxon signed-rank test [73] is employed, which is a nonparametric version of the paired student's t-test. Nonparametric statistical tests make fewer assumptions, such as not assuming that the distribution of the skill scores (e.g., the classification accuracy) is Gaussian. Therefore, it normally has more power when the expectations of the t-test are violated, e.g., independence.

As mentioned earlier, using the k-fold cross-validation intrinsically violates the statistical assumptions of observations being independent; hence, the McNemar's test [73] is alternatively used in this dissertation to compare the performance of different models. In contrast to the Wilcoxon method that uses the accuracies obtained from multiple runs of each classifier as statistical samples to compare the models, the McNemar's test is calculated based on a single-run classification, which leads to a single *p*-value per run. The McNemar's test operates on a contingency table calculated based on the predicted labels of each classifier.

CHAPTER 3

A Hierarchical Structure for Behavior Classification

In this chapter, a hierarchical classification structure is developed to perform the behavior classification from LFP signals through a multi-level framework. At each level, the time-frequency representations of all six contacts of the DBS leads are combined through an MKL-based SVM classifier to classify five tasks (speech, finger movement, mouth movement, target reaching, and random segments). To lower the computational cost, the inter-hemispheric synchronization of the LFPs is alternatively used to make three pairs out of six bipolar signals. Three classifiers are separately trained at each level of the hierarchical approach, which lead to three labels. A fusion function is then developed to combine these three labels and determine the label of the corresponding trial. Using all six LFPs with the proposed hierarchical approach improves the classification performance. Moreover, the synchronization-based method reduces the computational burden considerably while the classification performance remains relatively unchanged.

3.1 Introduction

In recent years, classification of the human behavior using LFP signals has been addressed in some studies, aiming at providing basis for behavior-adapted closed-loop DBS systems. Considering the oscillatory nature of the STN-LFPs, Loukas and Brown [18] proposed an algorithm to predict self-paced hand-movements. A pilot research was done by Santaniello et al., [13] in which a closed-loop DBS system capable of adjusting the stimulation amplitude was developed. The LFP signals from ventral intermediate nucleus (VIM) of the thalamus were used as the control variable in their closed-loop system. Time-frequency analysis of the β frequency range (~10-30 Hz) of the LFP signals has been used in different studies [40,41] to drive SVM or multiple kernel learning (MKL)-based SVM classifiers for human behavior recognition purposes. An adaptive learning approach using LFP signals was proposed in [44], where the authors developed a hybrid model for human behavior clustering based on combining SVM and hidden Markov model (HMM). In [45], a non-linear regression method was developed to measure the inter-hemispheric connectivity between LFP signals, aiming at detecting motor activity, like finger movement of the PD patients.

In this chapter, we focus on human behavior classification using LFP signals recorded from the STN regions of the brain. The wavelet decomposition of the acquired signals within the β frequency range is used to generate a more distinctive feature space for representing different human behaviors [1,74]. In contrast to the previous work [40,41] in which just a single or a pair of the bipolar signals are employed in the classification step, it is proposed to utilize all recorded bipolar LFP signals (three bipolar LFP signals are

recorded from each STN using all four contacts of implanted DBS leads, resulting in six bipolar LFP signals from two STNs) to feed an MKL-based SVM classifier for behavior recognition purposes. A hierarchical structure capable of performing the behavior classification at different levels of resolution, ranging from a coarse level (e.g., action recognition) to a finer level (e.g., a sub-category of the motor activity, like finger movement) is developed. Such a coarse-to-fine scheme provides a flexible classification interface that can easily be terminated at each level of resolution defined by the user. As a consequence, it enhances the discrimination ability of the classifier since a fewer number of classes requires to be analyzed at each level.

However, using all six available LFPs potentially tends to increase the computational burden due to the size of the feature vectors. To overcome this problem, a classification scheme is alternatively proposed that takes advantage of all available data at each level of the hierarchical scheme while the computational burden still remains low. To this end, considering the synchronized aggregate activity of the LFP signals acquired from the basal ganglia [75-78] and inspired by the classification method presented in [41], an FFT-based synchronization approach is used to pair up the recorded LFP signals, making three pairs out of six available signals for each trial and driving three classifiers. Finally, three predicted labels of a single trial are fused through a decision function to estimate the label of the input trial at each level of the hierarchical scheme. With this approach, the computational burden decreases considerably while the classification performance remains relatively unchanged.

The remainder of this chapter is organized as follows: first, the proposed methods are explained. The experimental results and quantitative assessments are given afterwards. The chapter ends with conclusions and some remarks.

3.2 Methodology

In this section, the proposed hierarchical classification structure is first introduced, which is capable of classifying human behavior at different levels by combining all six available bipolar LFPs through an MKL-based SVM classifier. Then, a principled method based on an FFT-based synchronization of the LFPs is explained to reorganize six acquired signals of each trial. As a result, an alternative data selection method is developed that takes advantage of all six LFPs for classification step but in a different implementation scheme.

3.2.1 Hierarchical Classification Scheme

As mentioned earlier, the Lp-norm MKL classifier was previously applied on the STN-LFP signals for human behavior classification purposes [40,41]. Here, a hierarchical classification approach is developed, which in contrast to the existing methods is capable of performing classification at different levels of resolution. With this approach, a top-down classification scheme is developed in which the input LFP signals are categorized into two major classes at the first level, including “action” and “random” classes. With the random class, we refer to those parts of the recorded signal where the subject is in the rest position and no specific activity is done. The reason behind using the random segments is to train the classifier to recognize other tasks rather than the defined ones. Note that, if the entry is classified as the random signal, the classification is terminated at the first level. On

the other hand, the classification may continue at a finer level if there is a sub-category for the classified sample, and the user desires to classify the input sample in more details to further explore the label of the corresponding trial (e.g., motor, non-motor, and etc.). Such a coarse-fine classification procedure is depicted in figure 3.1 by a tree-like structure.

To proceed with the training phase of the classifier based on the proposed hierarchical structure, the samples from different sub-categories at finer levels should be combined at coarser levels, necessitating a bottom-up procedure to form the training samples. For instance, in terms of the "Dataset1" used in this work, the "button press", "mouth movement", and "target reaching" trials at the third level are combined to generate the training samples for the "motor" activity at the second level. Clearly, all the existing activities including "motor" and "speech" should be combined at the first level to generate the samples belonging to the class "action" versus the class "random".

3.2.2 Synchronization-based Approach

This section presents an alternative channel selection approach that still uses all six bipolar LFP channels of each trial but with a different realization. To this end, an FFT-based synchronization method [79] is employed to pair up the bilateral LFP channels. Thus, we first briefly review the main characteristics of this method here, and, then, present our proposed scheme.

3.2.2.1 FFT-based Synchronization Method

The FFT-based synchronization approach has been used for different analytical applications of EEG and LFP signals such as source localization and classification [41,79]. It has been shown that some of the acquired LFP signals are inherently less informative

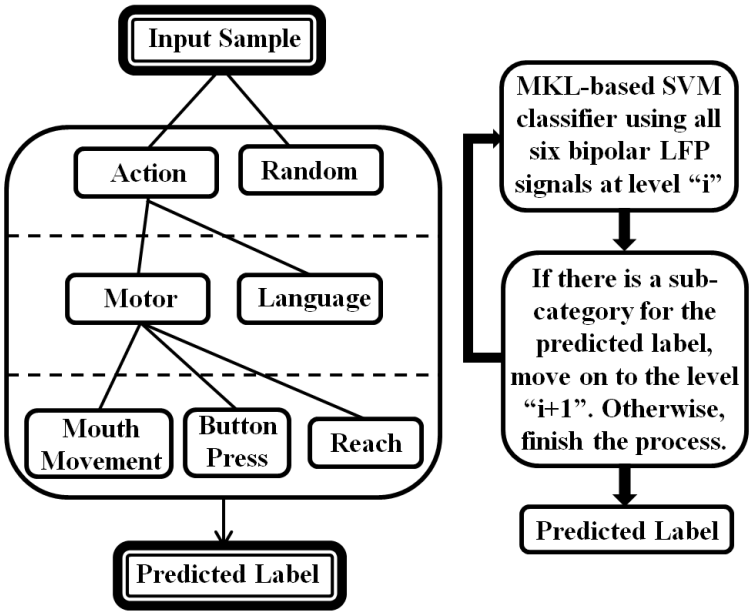

Figure 3.1. The proposed hierarchical structure for behavior classification. Left shows an example of a three-level classification scheme in a top-button design. Right shows the block diagram of the classification procedure. If the classification is terminated at the first level, there is no loop and the predicted label is given as the output. Otherwise, the classification may continue at a finer level until there are no more sub-categories for the predicted label.

than others, likely due to their location in the sensorimotor area of the STN [41]. And, they are poorer candidates for other post-processing steps such as behavior classification. The FFT-based synchronization has been successfully employed in [41] to specifically address the problem of selecting the more informative LFP signals recorded from STNs.

A typical time-domain signal contains different phase values associated with the frequency components of its Fourier expansion. Essentially, with the FFT-based synchronization method, the phase values of all frequency components are taken into account to obtain a more accurate measure compared to other statistical correlation-based methods [79].

Let x(t) be a continuous LFP signal acquired from one of the bipolar-referenced contacts of an implanted DBS lead, the Fourier representation of the signal and the corresponding phase components are given as follows:

$$x(t) = a_0 + \sum_{n=1}^{\infty} \left(a_n^2 + b_n^2\right)^{1/2} \sin\left(\omega_n t + \theta_n\right), \qquad (3.1)$$
$$\theta_{\mathrm{n}} = \tan^{-1}\left(\frac{a_n}{b_n}\right).$$

where, a_n and b_n are the Fourier coefficients of the signal $x(t)$ at the n^{th} frequency component and θ_n is the corresponding phase value.

The synchronization value between two signals $x_i(t)$ and $x_j(t)$ is calculated based on the phase difference at each frequency component of their Fourier representations. Accordingly, the main assumption is that if two signals are synchronous, their corresponding phase lag should be almost uniform across all harmonics. This implies that for two arbitrary frequency components *m* and *n* the phase difference of two almost phase-synchronous signals becomes [41,79]:

$$\left|\theta_{\mathrm{im}} - \theta_{\mathrm{jm}}\right| \approx \left|\theta_{\mathrm{in}} - \theta_{\mathrm{jn}}\right| \Rightarrow$$
$$\left|\frac{a_{im}b_{jm} - b_{im}a_{jm}}{a_{im}a_{jm} + b_{im}b_{jm}}\right| \approx \left|\frac{a_{in}b_{jn} - b_{in}a_{jn}}{a_{in}a_{jn} + b_{in}b_{jn}}\right|. \quad \forall m,n \qquad (3.2)$$

Consequently, both the mean and standard deviation of two consecutive phase lag values is a small quantity across all harmonics for two nearly synchronous signals. It means that, given $E(n)$,

$$E(n) = \left|\frac{a_{in}b_{jn} - b_{in}a_{jn}}{a_{in}a_{jn} + b_{in}b_{jn}} - \frac{a_{in+1}b_{jn+1} - b_{in+1}a_{jn+1}}{a_{in+1}a_{jn+1} + b_{in+1}b_{jn+1}}\right|. \qquad (3.3)$$

the value of the normalized phase synchronization in the range [0,1] is defined as the following equation:

$$sync(x_i(t), x_j(t)) = \frac{1}{1 + mean(E(n)) + std(E(n))}. \quad (3.4)$$

where, *mean*(·) and *std*(·) are respectively the average and standard deviation of the quantity *E*(*n*) calculated across all the frequency components. From this equation, one can conclude that the more phase synchronous two signals are the closer to 1 is the value of *sync*(·) and vice versa. Note that, one of the main advantages of the FFT-based synchronization approach is that its computational complexity is no more than the FFT algorithm itself.

3.2.2.2 Label Fusion Scheme

As described in Section 3.2.1, all LFP signals of each trial (i.e., six bipolar signals from two implanted DBS leads) are used to generate the corresponding sample for the classification stage. In our evaluations, it was observed that using all existing data improves the classification performance, but it leads to a higher computational cost due to the size of the input data.

To tackle this limitation, a synchronization-based classification approach along with a label fusion function is developed that takes advantage of all recorded bipolar LFP signals while no considerable computational cost is imposed. With our approach, the synchronization between all acquired bipolar LFP signals is used to pair them up, making three pairs out of six available bipolar signals for each trial. This process is done by using all existing bipolar LFP signals (three from left and three from right STNs) to calculate synchronization values, generating a 3×3 synchronization table with nine values (S11, S12,

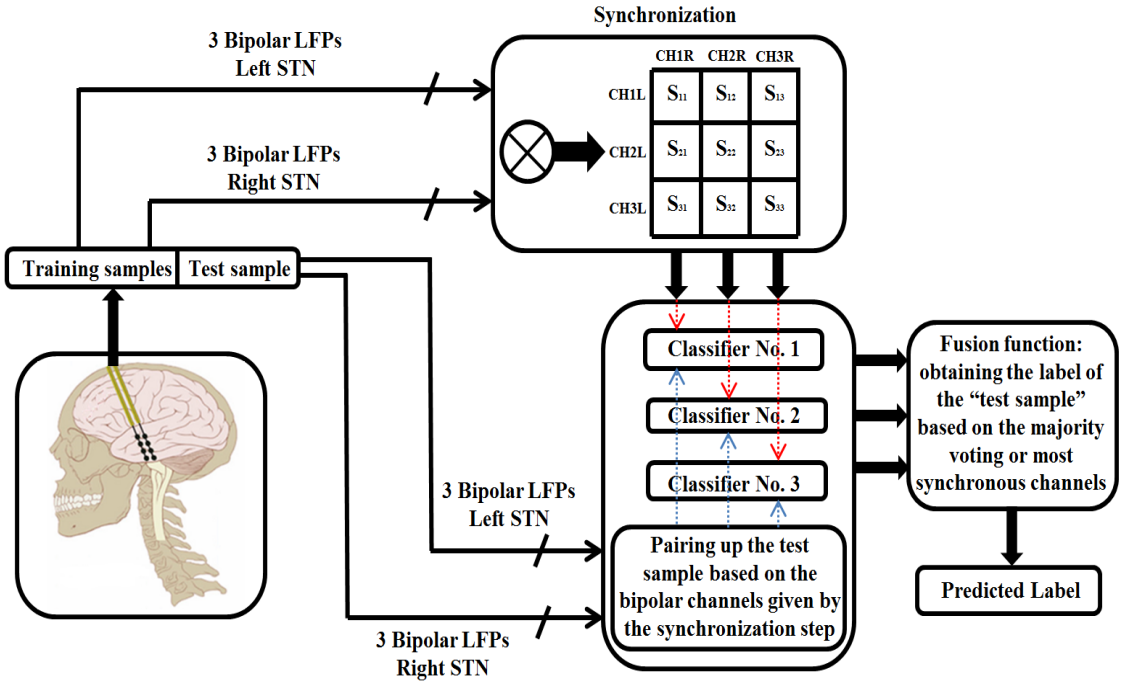

Figure 3.2. The proposed synchronization-based classification and label fusion scheme. As seen, the synchronization of all six available LFP signals (three from left STN and three from right STN) is first calculated. Then, three separate classifiers are trained based on the selected bipolar LFP signals. The label of the test sample is obtained through a majority voting approach. Note that, when all predicated labels are different, the label obtained by the most synchronous channel is considered as the final label.

…, S33) as shown in figure 3.2. Afterwards, for each of the left bipolar LFPs the corresponding LFP signal from the right STNs that obtains the maximum synchronization value is chosen to make a single left-right pair, e.g., CH1L-CH2R. This procedure is performed for all three left LFPs to get the most synchronous LFP signal from the right STN, making three left-right pairs for the classification purpose.

As a consequence, three classifiers are separately trained, leading to three labels for each input trial. In ideal cases, these three labels should be the same since they come from a single test sample representing a specific behavior. This implies that a majority voting approach is used as the label fusion function to obtain a single label for the corresponding input trial. However, a critical situation may occur when all three predicted labels are

different. This may happen since some of the bipolar channels are inherently less informative, leading to inappropriate data for classification purposes. To address such a tie situation, the label resulted from the most synchronous pair of the LFP signals is used as the final label. This is consistent with the results reported in [41], where it was shown that the most synchronous channels are most informative, providing reliable data for the classification purposes. Figure 3.2 shows the proposed synchronization-based classification scheme and the label fusion function graphically.

With the above-described approach, all the available LFP signals associated with each trial are used for the behavior classification, but in a way determined by the synchronization approach. In other words, a compromise between the most synchronous pair of the LFP signals and two other pairs is provided such that a better behavior classification performance is achievable. As it will be shown in Section 3.4, the quantitative results of this method are comparable to those obtained by combining all six bipolar LFP pairs in a single classification problem. However, through this approach, the computational burden still remains low.

In the rest of this chapter, we refer to the proposed method using all six LFPs combined at each level of the hierarchical structure as “HirAll”. Moreover, when the term “HirFus” is used, it means that the synchronization-based classification scheme and label fusion are used at each level of the hierarchical structure.

3.3 Experiments and Results

To evaluate the performance of the proposed method in classifying human behavior, two separate datasets (Dataset2 and Dataset3), including eight PD subjects underwent DBS

surgery are used in our experiments (see Section 2.1). All the subjects were able to comply with the experimental paradigm. We excluded trials from our experiments when the subjects failed to respond to the cue signals timely (i.e., the timing cutoff was 2 sec).

As shown in [1,40,41], the time-frequency representation of the LFP signals can best discriminate different human behavior, improving the classification performance. Hence, the spectrogram of the raw LFP signals are first calculated to generate the feature space for the input samples. To this end, using the complex Morlet wavelet, the amplitude of the time-frequency components of the acquired data are calculated inside a window defined around the onset of each trial. In our experiments, this window includes the wavelet coefficients of the β frequency range (f~10-30Hz) calculated within an interval (-1,1) sec around each onset. To keep the computational burden low, these feature vectors are down-sampled by a factor of 100, and, then, PCA is applied on them before exposing the data to

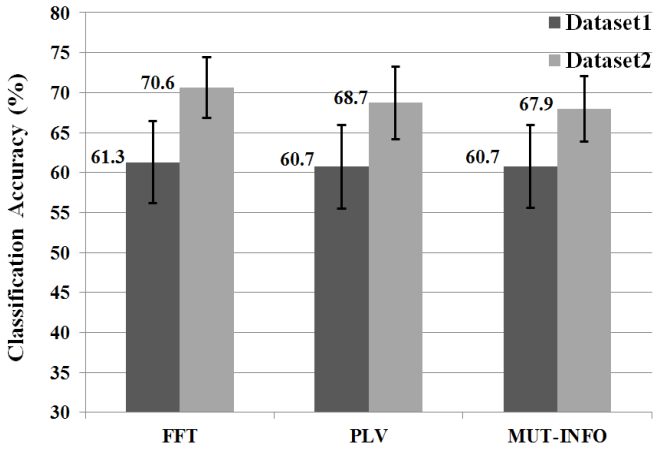

Figure 3.3. Comparison of the impact of the FFT, PLV, and Mutual information (MUT-INFO), synchronization methods on pairing up the bipolar LFP channels and the classification performance of the proposed HirFus approach using MKL-based SVM classifier. As seen, the FFT-based approach is slightly trending to better classification performance.

the classifier. In our experiments, 95% of the eigenvalues corresponding to the maximum variance direction is kept with the PCA calculations.

As described in Section 3.2.2, an FFT-based synchronization method is used to analyze the recorded LFP signals and pair them up for the classification purposes. Inherently, the FFT-based synchronization approach takes into account the phase difference between respective frequency components of the time sequences, leading to a more accurate approach in comparison with statistical-based synchronization methods [79]. To calculate the Fourier coefficients, no overlapping window is used in our analysis; rather, the FFT algorithm is run using a single window containing the input data.

It is worthwhile to evaluate the impact of different synchronization approaches on the classification accuracy. Figure 3.3 depicts the effect of the phase locking value (PLV) [80], mutual information [81,82], and the FFT [79] methods on the classification performance of the proposed HirFus approach using MKL-based SVM classifier. As seen, the

Table 3.1. Comparison of different classification approaches using Dataset2. The best classification accuracy, (mean $\pm$ std)%, is highlighted in each column. the abbreviations "BP", "MM", "SP", "RE", and "RA" respectively stand for "button press", "mouth movement", "speech", "reach" and "random" trials. the classifier used in each case is given inside the parentheses.

	5-class classification (BP, MM, RE, SP, RA)	Second Level (Speech, Motor, Random)	First Level (Action vs Random)
SVM (Linear)	49 ± 7	N/A	N/A
SVM (RBF)	54 ± 8	N/A	N/A
MKL-based SVM	57 ± 5	N/A	N/A
HirFus (SVM (Linear))	55 ± 5	60 ± 5	70 ± 2
HirFus (SVM (RBF))	55 ± 4	58 ± 4	70 ± 4
HirFus (MKL-based SVM)	61 ± 5	64 ± 4	73 ± 3
HirAll (SVM (Linear))	61 ± 7	64 ± 7	75 ± 5
HirAll (SVM (RBF))	50 ± 5	51 ± 5	66 ± 4
HirAll (MKL-based SVM)	$\mathbf{64 \pm 4}$	$\mathbf{67 \pm 4}$	$\mathbf{75 \pm 6}$

Table 3.2. Comparison of different classification methods using Dataset3. The best classification accuracy, (mean ± std)%, is highlighted in each column. the abbreviations "BP", "SP", and "RA" respectively stand for "button press", "speech" and "random" trials. the classifier used in each case is given in the parentheses.

	3-class classification (BP, SP, RA)	First Level (Action vs Random)
SVM (Linear)	63 ± 10	N/A
MKL-based SVM	64 ± 9	N/A
HirFus (SVM (Linear))	68 ± 2	71 ± 2
HirFus (MKL-based SVM)	71 ± 4	76 ± 4
HirAll (SVM (Linear))	77 ± 5	79 ± 3
HirAll (MKL-based SVM)	$\mathbf{78 \pm 6}$	$\mathbf{82 \pm 4}$

classification accuracy is almost equal when the aforementioned methods are used for pairing the bipolar LFP signals. For instance, the range of obtained classification accuracies is ~0.5% and ~2.5% respectively for Dataset2 and Dataset3. As a consequence, one can conclude that all these synchronization methods are approximately employing the same bipolar LFP channels for post-processing steps as well as classification. However, as shown in figure 3.3, the FFT-based synchronization is trending to better classification performance. Therefore, this method have been employed to develop our HirFus approach.

3.3.1 Classification Performance

This section compares the classification performance of the presented HirFus and HirAll methods with some other classifiers recently proposed for human behavior classification purposes using LFP signals [40,41]. The effect of various kernel functions on the classification performance is also examined in our experiments, including linear $k(\mathbf{x}, \mathbf{y}) = \mathbf{x}^{\mathrm{T}}\mathbf{y}+c$, polynomial $k(\mathbf{x}, \mathbf{y}) = (\mathbf{x}^{\mathrm{T}}\mathbf{y}+c)^{d}$, and RBF $k(\mathbf{x}, \mathbf{y}) = exp(\gamma\|\mathbf{x}-\mathbf{y}\|^2)$ kernels [66], where $\mathbf{x}$ and $\mathbf{y}$ are two feature vectors, and γ, c, and d are optional constants. In all experiments, a leave-one-out cross validation (LOOCV) approach is used to form the

training and test sets in our assessments [64]. Moreover, in case of the Lp-norm MKL-based SVM classifier, the parameters C and p are set to C=100 and p=1.5 to achieve the suitable classification performance.

Tables 3.1 and 3.2 respectively show a comparison of different classification methods in recognizing the human behavior for Dataset2 and Dataset3. The average and the standard deviation of the classification accuracies ($mean \pm std$)% obtained from all subjects and methods are given in these tables. As can be seen, the proposed HirAll method achieves the best results in almost all cases. The HirFus approach shows very competitive results to those obtained by the HirAll. However, as mentioned earlier, it outperforms the HirAll in terms of the computational cost.

An interesting cross-method comparison can be done for 5-class (Dataset2) and 3-class (Dataset3) classification cases. As can be observed from the left column of Tables 3.1 and 3.2, both the proposed HirAll and HirFus approaches achieve higher classification

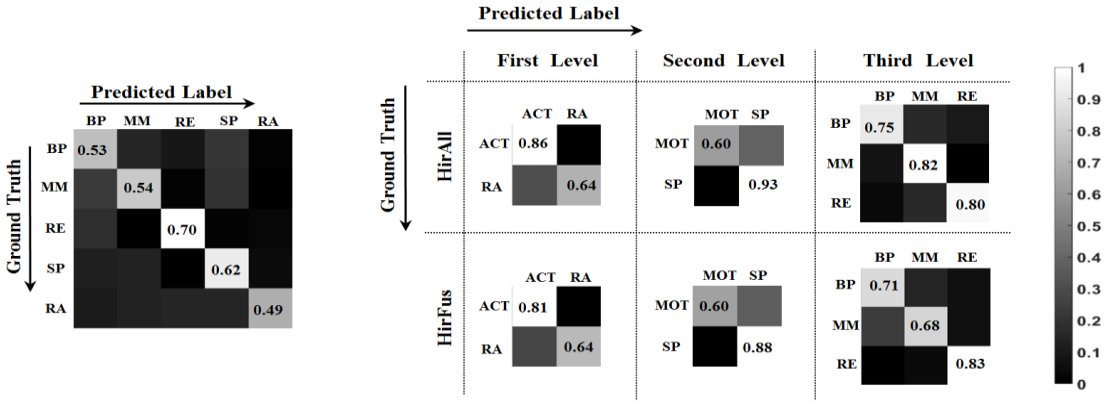

Figure 3.4. Average confusion matrix of all subjects of Dataset1. Left shows the confusion matrix of the single-level MKL-based SVM classifier. Right top and bottom rows respectively show the confusion matrix of the proposed HirFus and HirAll approaches at each level of the hierarchical structure.

performance than other methods. For example, while the MKL-based SVM classifier achieves $(57 \pm 5)\%$ accuracy with Dataset2 and 5-task classification, the accuracy of this classifier is $(64 \pm 4)\%$ and $(61 \pm 5)\%$ with the proposed HirAll and HirFus approaches respectively. The same performance is obtained when the hierarchical structure is used with the SVM classifier. For instance, the SVM classifier achieves $(61 \pm 7)\%$ and $(55 \pm 5)\%$ respectively using HirAll and HirFus approaches whereas the classification accuracy of the single-level SVM classifier is $(49 \pm 7)\%$.

The results obtained by Dataset3 are given in Table 3.2. As seen, the MKL-based SVM classifier reaches an accuracy of $(64 \pm 9)\%$ for 3-class classification. On the other hand, the proposed HirAll and HirFus methods earns $(78 \pm 6)\%$ and $(71 \pm 4)\%$ respectively.

The average confusion matrices of different classification modalities are shown in figure 3.4, including the single-level MKL-based SVM classifier, and the proposed HirFus and HirAll methods (for the sake of brevity, the confusion matrix of Dataset2 is only shown in figure 3.4). As seen, the maximum recognition rate of the single level classification belongs to the "reach" category by 70%, while the "button press" and "mouth movement" categories have roughly the same accuracy.

In contrast to the single-level classification approach that gives a specific recognition rate for each class, the proposed hierarchical structure can lead to different recognition rates, depending on the level of resolution defined for the classification to proceed. For instance, if the classification procedure is terminated at the first level of "Action" versus "Random" recognition, the accuracy rates of the "Action" label are 86% and 81%, respectively for the proposed HirAll and HirFus methods.

3.3.2 Computational Cost

As shown in Tables 3.1 and 3.2, the HirAll approach relatively surpasses the HirFus in terms of the classification accuracy. However, it is worth comparing the computational cost of different methods to gain insight into their full capability. A suitable trade-off between the computational burden and the classification accuracy gives the best setup, which can be determined by some restrictions such as power consumption and computational time in hardware implementation.

To compare the execution time, all algorithms were coded in MATLAB 2013a (Mathworks Inc., Natick, MA, USA), 64 bit version. All experiments were done on a PC with an Intel core i5 processor (3.4GHz) and 8GB of memory. When a test sample comes up for classification, three major processing steps need to be done: time-frequency calculation in the β frequency range, PCA, and label prediction. Note that all the information concerning the synchronization and pairing the bipolar LFPs are given from the training phase. Therefore, it is not needed to perform any calculations regarding the synchronicity of LFP channels for the corresponding test sample. The approximate execution time of the HirAll is given as follows: 1200ms for the calculation of the spectrograms of six recorded bipolar LFP signals (three from the left STN and three from right STN), 2.4ms for the PCA calculation, and 6.5ms for the label prediction. However, the computational time of the same steps for the HirFus are as follows: 400ms for the calculation of spectrograms (two spectrograms for each classifier in a pair-wise configuration), 0.6ms for the PCA calculation, and 4.2ms for the label predication.

3.3.3 Statistical Analysis

Apart from the computational cost, it is worth comparing the proposed HirFus and HirAll methods statistically to find out if their classification ability differs significantly. To this end, the aforementioned methods were run 50 times with randomly selected training and test sets (3-level classification was used). The McNemar's statistical test (see Section 5.2) was applied on the results of each run to compare the classification performance between two methods. As a result, 50 *p*-values were obtained for 50 runs while comparing the HirFus and HirAll algorithms. The experimental results showed that only 6 out of 50 calculated *p*-values were less than the 0.05 significance level, meaning that the difference between the HirFus and HirAll classification methods were not statistically significant.

3.4 Summary

The main objective of this chapter was to develop a new method for classification of human behavior using LFP signals recorded from STN regions of the brain, providing insights for deciphering the intraoperative neural signals in STN DBS response. Recognition of human behavior using different brain signals plays an important role in designing the next generation of the closed-loop behavior-adapted DBS systems as well as brain-computer interfaces.

The raw LFP data were recorded from all four contacts of each DBS lead implanted in the left and right STNs, resulting in six bipolar referenced LFP signals during the recording sessions. The proposed classification method was rooted on the time-frequency analysis of the acquired signals in the β frequency range (~10-30 Hz). A hierarchical structure was

proposed to perform the behavior classification via a multi-level framework, which was able to recognize human behavior at different levels of resolution ranging from a coarser level, like action recognition to a finer level, like finger movement. An Lp-norm MKL-based SVM classifier was employed for behavior classification task at each level of the proposed hierarchical approach.

Different combinations of the recorded LFP signals were employed with the introduced classification scheme. First, all LFP signals were combined via the MKL formulation to recognize the label of the corresponding trial. In spite of its suitable performance, such a method increases the computational burden due to the size of the feature vectors.

To reduce computational costs, a feature selection method was alternatively developed that still incorporated all recorded LFP data using a pair-wise strategy. An FFT-based phase synchronization approach was used to form three interhemispheric pairs out of six available bipolar LFP signals. Three classifiers were then driven at the same time, leading to three labels for the corresponding trial. Finally, these labels were passed through a fusion function to determine a single label for the input trial. With this approach, the computational performance increased significantly while the classification accuracy fell slightly.

Various experiments were carried out on two separate datasets including the LFP signals recorded from nine subjects undergoing DBS surgery. Different behavioral tasks including button press, mouth movement, speech, target reaching, and random segments were considered in our assessments. We compared the classification performance of our proposed HirFus and HirAll methods against some state-of-the-art methods used for the

human behavior recognition based on the LFP signals. The quantitative results confirmed the superiority of our approaches in almost all cases. Moreover, in all evaluations, regardless of the employed classifier, applying the hierarchical structure improved the classification performance, showing the effectiveness of the proposed approach.

CHAPTER 4

LFP-Net; A Deep Learning Framework for Behavior Classification

This chapter presents LFP-Net, an automated machine learning framework based on deep convolutional neural networks (CNN) for classification of human behavior using the time-frequency representation of STN-LFPs within the beta frequency range. CNNs learn different feature maps based on the beta power patterns associated with different behaviors. The features extracted by the CNNs are passed through fully connected layers and then to the softmax layer for classification. Our experiments on ten PD patients performing different behavioral tasks show that in most cases the proposed LFP-Net outperforms other state-of-the-art classification methods. Moreover, compared to well-known deep neural networks such as AlexNet, LFP-Net gives a higher accuracy using significantly fewer parameters.

4.1 Introduction

Most recently, deep neural networks (DNN) have gained considerable attention for numerous classification and regression tasks. A deep belief network (DBN) model was proposed by [35] for binary motor imaginary (MI) classification and obtained better

performance compared to SVM. DBN has also been used in other related studies for anomaly measurement of EEG signals [36]. Convolutional neural network (CNN) was used to classify MI using EEG signals [37]. CNN and stacked auto-encoders (SAE) was used to classify EEG MI signals [38].

As mentioned earlier, recognition of the human behavioral activities using the sensed bio-signals is one of the key steps in designing the next generation of closed-loop systems as well as BCIs. This chapter aims to study the capability of the SNT-LFP neural feedbacks in distinguishing basic human activities such as motor and speech tasks. This study provides grounds for developing more complicated behavior recognition algorithms capable of identifying a broader spectrum of behavioral tasks, paving the path toward the long-term goal of designing behaviorally adaptive closed-loop DBS systems. In contrast to

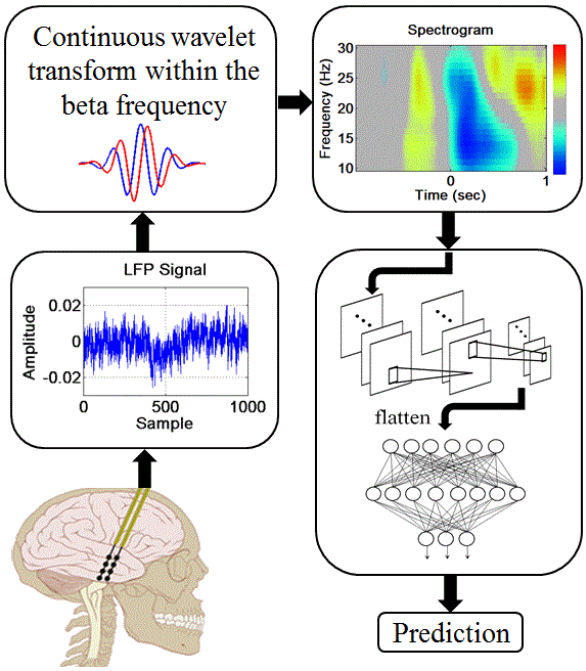

Figure 4.1. The schematic of the proposed classification method.

the latest efforts that mainly focused on turning the stimulation pulse “on” and “off”, the behavior-adapted systems would be able to identify the patients’ current state to modulate a customized stimulation signal consistent with the patients’ need.

In this chapter, a deep learning framework is introduced for automatic classification of human behavior using STN-LFP signals. To the best of our knowledge, it is the first time that a deep learning framework is developed using STN-LFP signals for a behavior classification task. The beta frequency components (f~10-30 Hz) of the time-frequency representation (spectrogram) of the acquired raw LFPs are used to distinguish different behavioral tasks. Figure 4.1 shows the schematic of the introduced method.

The proposed deep neural network framework is composed of six 2D convolutional layers, batch normalization units, and three max-pooling layers. The obtained feature map from these layers is followed by two fully connected layers to finally drive a softmax activation function, assigning a class label to each input spectrogram. In contrast to other existing classification methods [39-43] that address the behavior classification task using engineered features and traditional classifiers such as SVM, here, a deep neural network architecture is proposed to learn the feature space. To evaluate the classification performance of the proposed method as well as other related state-of-the-art classification approaches, three separate datasets containing different behavioral tasks are employed (see Section 2.1). Our experiments show that the proposed deep learning approach significantly outperforms other compared methods in terms of classification accuracy.

The rest of this chapter is organized as follows: Section 4.2 elaborates on the proposed method. Section 4.3 discusses the experimental results and analysis. Finally, Section 4.4 concludes the chapter with some discussions.

4.2 Methodology

This section presents the proposed deep learning architecture for the classification of human behavior using the STN-LFP signals. As mentioned earlier, the time-frequency representation (spectrogram) of the raw LFP signals in the beta frequency range is used as input to feed the network for training, validation, and test phases. The Z-norm normalization is applied on each spectrogram based on a 0.5 sec window prior to the initiation of each trial. Note that the trial initiation is aligned to a "cue" beep given to

Table 4.1. Summary of the proposed LFP-Net architecture given by the Keras deep learning library

Type of layers	Size of the feature map at the output of each layer	Size of the convolutional filter	Filter stride	Number of parameters
Convolutional+ ReLU	(254×254×24)	(3×3)	(1×1)	240
Batch-normalization	(254×254×24)	N/A	N/A	96
Convolutional+ ReLU	(252×252×48)	(3×3)	(1×1)	10416
Max-pooling	(126×126×48)	N/A	N/A	0
Batch-normalization	(126×126×48)	N/A	N/A	192
Convolutional+ ReLU	(124×124×48)	(3×3)	(1×1)	20784
Batch-normalization	(124×124×48)	N/A	N/A	192
Convolutional+ ReLU	(122×122×24)	(3×3)	(1×1)	10392
Max-pooling	(61×61×24)	N/A	N/A	0
Batch-normalization	(61×61×24)	N/A	N/A	96
Convolutional+ ReLU	(59×59×24)	(3×3)	(1×1)	5208
Batch-normalization	(59×59×24)	N/A	N/A	96
Convolutional+ ReLU	(57×57×48)	(3×3)	(1×1)	10416
Max-pooling	(28×28×48)	N/A	N/A	0
Batch-normalization	(28×28×48)	N/A	N/A	192
Flatten	37632	N/A	N/A	0
Fully connected layer	64	N/A	N/A	2408512
Drop-out	64	N/A	N/A	0
Batch-normalization	64	N/A	N/A	256
Fully connected layer	3	N/A	N/A	195

subjects by a laptop computer inside the experimental environment. All the timing information is precisely recorded and synchronized to the LFP time sequence during each data recording session.

Table 4.1 gives a summary of the proposed LFP-Net architecture including all layers, the size of inputs and outputs of each layer, and the number of trainable parameters. Figure 4.2 shows a graphical representation of the proposed architecture. As seen, the proposed architecture includes six 2D convolutional layers (24, 48, 48, 24, and 48 filters respectively from layer one through layer six), seven batch-normalization units, three max-pooling layers, and two fully connected layers (including 64 and 3 units) with 50% dropout. In Section 4.3.3, it is discussed how the performance of the LFP-Net is affected by the change of the number of convolutional filters and convolutional layers. It is shown that the proposed architecture marginally leads to higher performance.

The shape of the input spectrograms is (height = 256, width = 256, channels = 1). The input of each layer is convolved with filters of size (3×3) to output the corresponding feature maps. Different numbers of filters are used for each convolutional layer, which

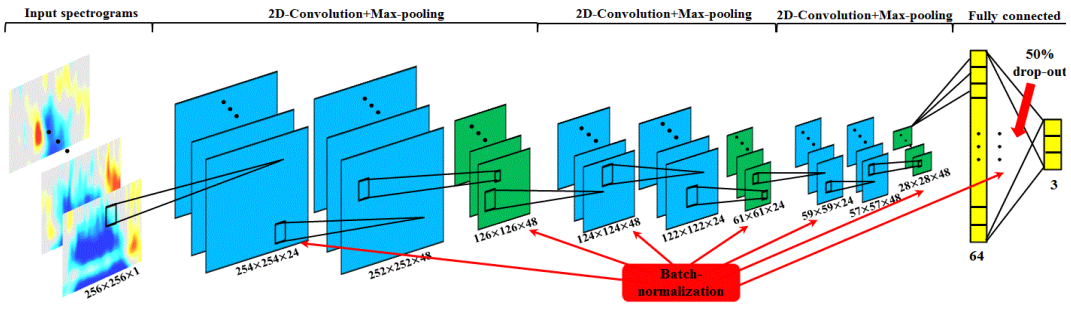

Figure 4.2. The architecture of the proposed LFP-Net. Inputs include the spectrograms associated with each trial. The network contains six convolutional+ReLU layers (blue boxes), three max-pooling layers (green boxes), and two fully connected layers (yellow box). The batch normalization (red box) is applied after each layer as shown by red arrows. The dimension of feature maps is given next to each layer.

their weights and biases are trained using the back-propagation procedure. The max-pooling operation takes place after the second, fourth, and sixth convolutional layers as shown in figure 4.2. The size of the max-pooling is (2×2), so the height and width of the input feature map are reduced by half after each max-pooling step. Finally, the input spectrogram of size (256×256×1) is converted to a feature map of size (28×28×48) after six convolutional layers and three max-pooling layers (see Table 4.1). The feature maps are then flattened and fed to two back-to-back fully connected layers with 64 and 3 neurons, respectively. The last unit has three neurons to address the 3-class classification task under consideration in this chapter: button press, target-reaching/speech, and random signal (the random segment is used to make the classifier learn how to distinguish between an activity and the rest state). Note that, Dataset2 given in Table 2.1 contains four behavioral activities; however, for the sake of consistency with Dataset1 and Dataset3, we only use the "button press" and "target-reaching" behavioral activates alongside the "random" trial for Dataset2 to address a 3-class classification problem. Later on, we separately evaluate the classification performance with all existing behavioral activities of Dataset2 in Section 4.6 (Appendix).

Two types of activation functions are used in this work: (1) rectified linear unit (ReLU) and (2) softmax [69]. After each convolutional layer, it is common to employ an activation function to add nonlinearity to the network structure. ReLU is a well-known activation function used for deep learning applications; hence, it is used here:

$$f(x)=\begin{cases} x & if\ \ x>0 \\ 0 & o.w. \end{cases} \tag{4.1}$$

Moreover, the output layer employs the softmax activation function to compute the probability distribution of output classes. In other words, a class label is allocated to the input data based on the maximum probability calculated by the softmax function. In terms of a *k*-class classification task, the softmax function gives a probability P_i to each input x_i as follows [69]:

$$P_i = \frac{e^{x_i}}{\sum_{j=1}^{k} e^{x_j}}, \qquad i = 1,2,\ldots,k \tag{4.2}$$

Finally, the cross-entropy loss function and Adam optimizer [83] is used to update the trainable variables through the backpropagation procedure.

4.3 Experiments and Results

This section presents the results of behavior classification experiments using STN-LFP signals with the proposed LFP-Net as well as comparisons with other classifiers.

4.3.1 Data Description and Classification Details

To evaluate the classification performance of the proposed LFP-Net, three different datasets is employed in our experiments (10 subjects in total) as described in Section 2.1. All the subjects were able to comply with the experimental paradigm. We excluded trials from our experiments when the subjects failed to respond to the cue signals timely (i.e., when the timing cutoff was more than 2 sec).

The performance of the LFP-Net is compared against the recently proposed approaches developed for behavior classification [39] using the STN-LFP signals. The classification performance of the proposed method is also compared with the AlexNet [69], which is a

well-known deep neural network architecture for classification purposes. The time-frequency representation of the raw STN-LFPs is calculated based on the amplitude of the CWT. A time-window of size (-1,1) sec around the onset of each trial is used to calculate the CWT. Moreover, the wavelet coefficients are calculated for the beta frequency range $f \sim (10–30)$ Hz, where the frequency resolution is chosen to be 0.25 Hz. Finally, the obtained spectrograms are resized to (256×256×1) before feeding them to classifiers.

The aforementioned time-window is defined based on the "onset" corresponding to each trial, which is recorded during the data acquisition sessions. For the random trials, however, random numbers are generated within the time span of the recorded LFP and used them as random onsets to obtain the random segments (time-window).

In all the experiments, 80% of the calculated spectrograms are randomly selected and used as the training set, 10% as a validation set, and the rest 10% as the test set. 10-fold cross validation is applied to the training and validation sets to obtain the best-trained model for each dataset, which is then applied on the test set to get the classification performance. As such, the cross-validation prevents overfitting. The details and specifications of each classifier are given as follows:

LFP-Net: the training phase is done using a batch size of 100, which specifies the number of spectrograms passed through the network for updating the weights using the backpropagation procedure. The network was trained for 30 epochs, meaning that the whole training set was passed through the network 30 times to compute the final weights for each cross-validation iteration. Considering the input size and the architecture of the

LFP-Net (see Table 4.1), the total number of trainable variables reported by the Keras neural network library [84] is equal to 2,466,723.

AlexNet: for the sake of consistency, the training phase of the AlexNet is done using the same number of batch sizes and epochs as given for the LFP-Net. The architecture of the AlexNet is as follows: it is composed of five 2D convolutional layers. The numbers of filters are 96, 256, 384, 384, and 384 respectively for these layers. The size of the corresponding filters is (11×11), (11×11), (3×3), (3×3), and (3×3). Also, ReLU activation function is applied after each convolutional layer, followed by a (2×2) max-pooling operation and batch normalization units. The extracted feature map is flattened and passed through four fully connected networks with 4096, 4096, 1000, and 3 neurons to output the class label of the entry. The "softmax" and "Adam" optimizer are applied to update the variables of the network in the same manner performed on the LFP-Net. The total number of trainable variables reported by the Keras is equal to 31,184,115.

SVM: in terms of the SVM classifier, the libsvm library is used [85]. All spectrograms are first converted to vectors before applying them to the SVM classifier. Moreover, the feature vector is down-sampled by a factor of 5 and apply the principal component analysis (PCA) dimensionality reduction to obtain the feature vectors for the SVM classifier. In our experiments, we observed that the dimensionality reduction and down-sampling remarkably improve the performance of the SVM classifier, which is consistent with other related work [40-43]. In our experiments, 95% of the eigenvalues corresponding to the maximum variance direction is kept with the PCA calculations. The effect of various kernel functions on the classification performance is also examined, including linear $k(x, y) =$

$x^T y + c$, and RBF $k(x, y) = \exp(-\|x - y\|^2)$ kernels [64,86], where x and y are two feature vectors, and c is an optional constant. The hyper-parameter of the SVM classifier 'C' is set to 1 in order to get the best performance.

4.3.2 Classification Performance

The classification ability of the proposed LFP-Net was compared against other methods in classifying human behavior using STN-LFPs. All the experiments were performed on a server machine with Linux operating system, Intel CI7 3.6 GHz processor, and 54 GB RAM. The proposed LFP-Net and AlexNet were implemented using Keras deep learning library and deployed on a GeForce GTX 1080 GPU with an 8 GB of memory.

Table 4.2 shows the classification accuracy (mean±std)% for all ten subjects of Datasets-1, 2, and 3 and all classifiers presented in Section 4.3.1. The reported values are calculated by repeating the experiments 50 times based on a random selection of the training, validation, and test sets and making an average of 50 repetitions.

Note that all experiments were done in a subject-dependent manner, meaning that the classifiers were trained and tested separately for each subject. This is due to the variability

Table 4.2. The classification accuracy (mean ± std) % of different classifiers. The results are reported for subjects 1-10 separately. The best value is highlighted in each column across all subjects. The weighted average of all 10 subjects is given in the rightmost column.

	Subjects										
Classifiers	1	2	3	4	5	6	7	8	9	10	average
LFP-Net	**89.4 (2.8)**	89.1 (2.3)	**84.7 (3.0)**	**84.7 (3.1)**	**92.1 (2.7)**	**85.87 (3.3)**	**91.2 (2.3)**	**88.3 (3.5)**	**93.7 (2.7)**	**85.3 (4.9)**	**88.3**
AlexNet	86.7 (4.2)	**91.1 (2.5)**	84.6 (2.7)	82.7 (3.4)	89.8 (2.3)	84.9 (3.4)	87.8 (3.0)	84.2 (3.1)	89.8 (3.5)	79.6 (4.4)	86.3
RBF-SVM	87.1 (3.2)	80.8 (3.2)	80.9 (2.8)	71.2 (3.7)	83.0 (2.7)	81.7 (2.8)	86.1 (2.5)	73.7 (2.7)	82.5 (3.6)	82.7 (3.3)	80.4
Linear-SVM	86.3 (3.8)	78.9 (3.1)	79.2 (2.9)	67.1 (3.8)	80.1 (3.1)	81.5 (3.0)	87.8 (2.9)	75.9 (3.7)	78.4 (3.1)	81.6 (4.0)	78.9

observed in the beta band power across different patients, probably because the surgical procedure cannot precisely place the clinical electrode in the same brain location across different patients. Further, even if the surgical procedure could precisely localize the lead in exactly the same neuroanatomical position, there is inherent variability in neuroanatomy across patients leading to different neural response.

As can be seen, the proposed LFP-Net outperforms other compared classifiers in almost all cases. The results of the AlexNet are competitive with the proposed method. However, in nine out of ten subjects the proposed method achieves better performance as compared to the AlexNet. It is worth mentioning that the number of trainable variables of the AlexNet is more than 31 million while the LFP-Net needs less than 2.5 million variables to be trained. As a result, the proposed method achieves higher performance with a remarkably lower computational cost. Figure 4.3 gives the training loss curves for LFP-Net and AlexNet. For the sake of brevity, the results of subject 1 (see Tables 2.1, 4.2) are only shown in this figure. As seen, the LFP-Net tends to quickly converge to the minimum loss near 0 with fewer fluctuations as compared to AlexNet. It suggests that the LFP-Net is a

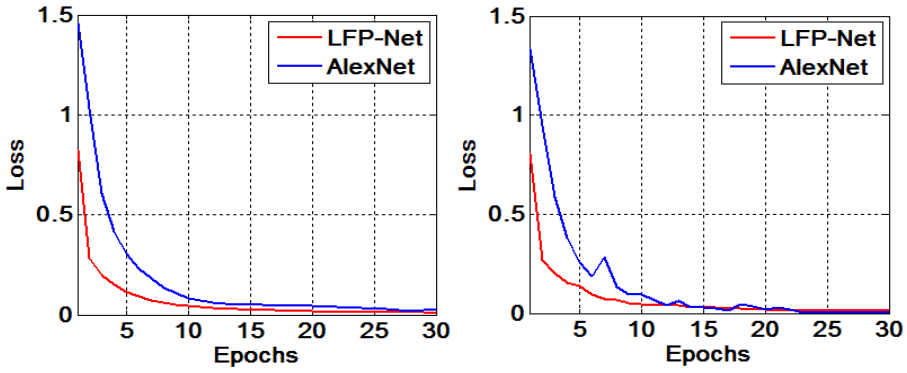

Figure 4.3. Comparison between the training loss of the LFP-Net and AlexNet. Left shows the average loss of 50 runs of LFP-Net (red) and AlexNet (blue) for subject 1. Right only shows the loss for one single run. The results are reported for the training set. As seen, the LFP-Net tends to faster convergence to the minimum loss near 0 with fewer epochs as compared to AlexNet.

more reliable architecture when working with a small training set (e.g., STN-LFP signals) since the network converges faster.

The classification accuracy given by the SVM classifier is less than the proposed method in all cases. Whereas the weighted average accuracy of all ten subjects with the RBF-kernel and Linear-kernel SVM classifier is about ~80%, the average accuracy of the proposed method is ~88%.

Figure 4.4 shows the weighted average confusion matrix of all subjects for the LFP-Net and AlexNet. As seen, the recognition rate of the proposed LFP-Net surpasses the AlexNet for Dataset2 and Dataset3 in all cases. However, AlexNet shows higher performance for Dataset1 only for “button press” and “target-reaching” classes, likely due to its higher classification performance on subject 2 (see Table 4.2). Apart from the classification accuracy, the sensitivity and specificity of two most competitive methods

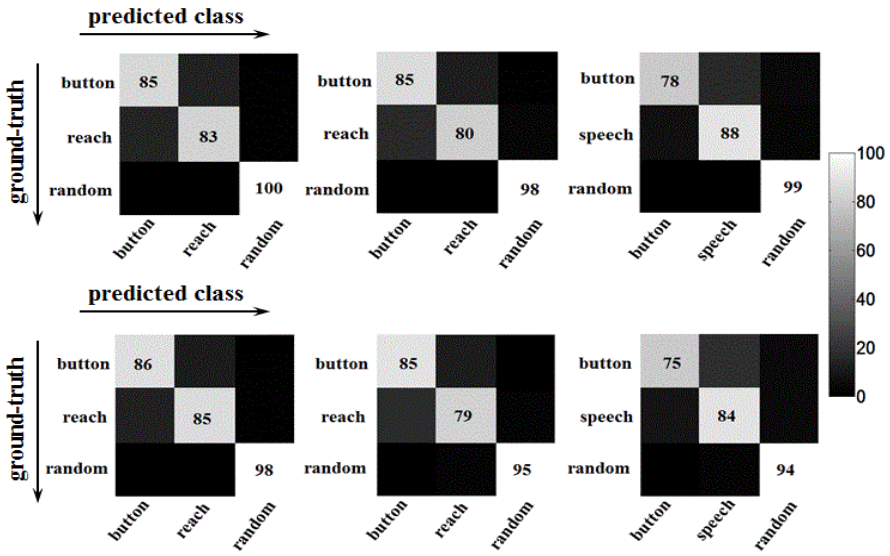

Figure 4.4. The confusion matrix of all subjects (the weighted average is shown in each case). The top row gives the results of the LFP-Net. The bottom row gives the results of the AlexNet. Left to right columns show the results obtained for Dataset1, Dataset2, and Dataset3, respectively.

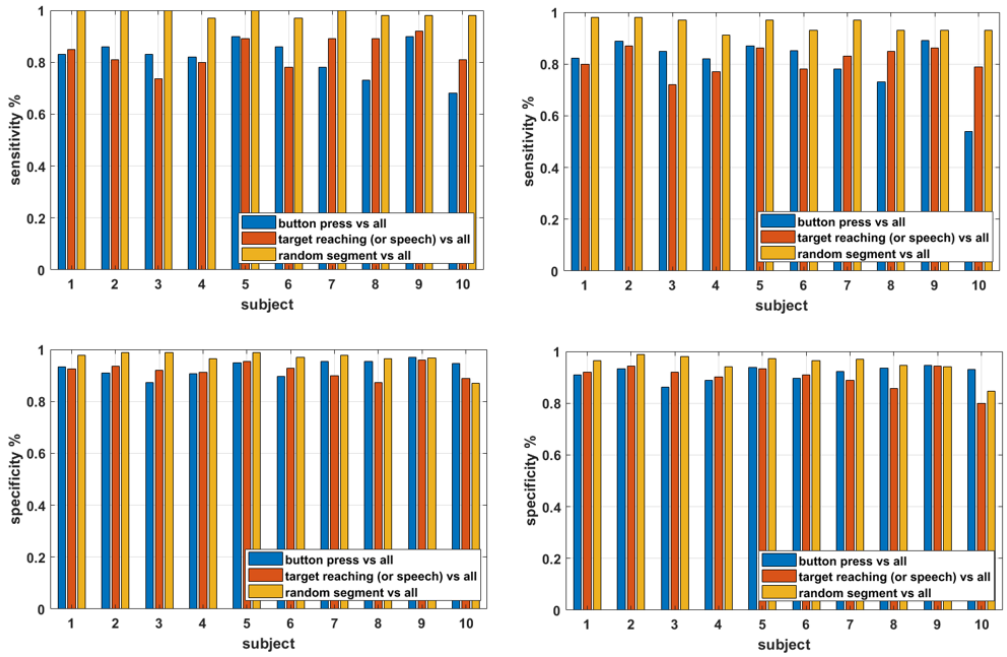

Figure 4.5. Sensitivity and specificity measures. Top row: comparison between the sensitivity of LFP-Net (left) and AlexNet (right). Bottom row: comparison between the specificity of the LFP-Net (left) and AlexNet (right).

(i.e., LFP-Net and AlexNet) is compared in figure 4.5. As shown, the LFP-Net surpasses in most of the cases by a few percent. Note that, since we have a multi-class classification problem, a one-vs-all approach was utilized to calculate the sensitivity and specificity measures in each case.

Furthermore, figure 4.6 illustrates the feature maps extracted at each layer of the LFP-Net for typical “button press” and “speech” trials, which helps assess how the feature maps change at different layers of the network.

4.3.3 Statistical Analysis

As presented earlier, all experiments are repeated 50 times by selecting a random set of training and test sets. As a result, it enables us to perform a statistical analysis on the classification accuracies in order to evaluate how significant their differences are.

First, Wilcoxon signed-rank test [73] is employed. Table 4.3 gives the p-values obtained by comparing each pair of classifiers under consideration using the 50 skill scores (classification accuracy). As shown, in seven out of ten subjects the LFP-Net is significantly better than the AlexNet (p-value < 0.05) while AlexNet is only performing better for subject 2. Compared to the SVM classifier, regardless of the kernel function, the proposed approach outperforms significantly in all cases.

As mentioned earlier, using the k-fold cross-validation intrinsically violates the statistical assumptions of observations being independent; hence, the McNemar's test [73] is alternatively used to compare the performance of different models. As a result, 50 p-values are obtained for 50 runs. Table 4.4 shows the number of p-value < 0.05 over 50 runs for each case. As can be seen, based on the McNemar's test, the classification power of the LFP-Net and AlexNet are not statistically significant; however, as mentioned earlier, the LFP-Net obtains higher classification accuracy in 9 out of 10 subjects with much less

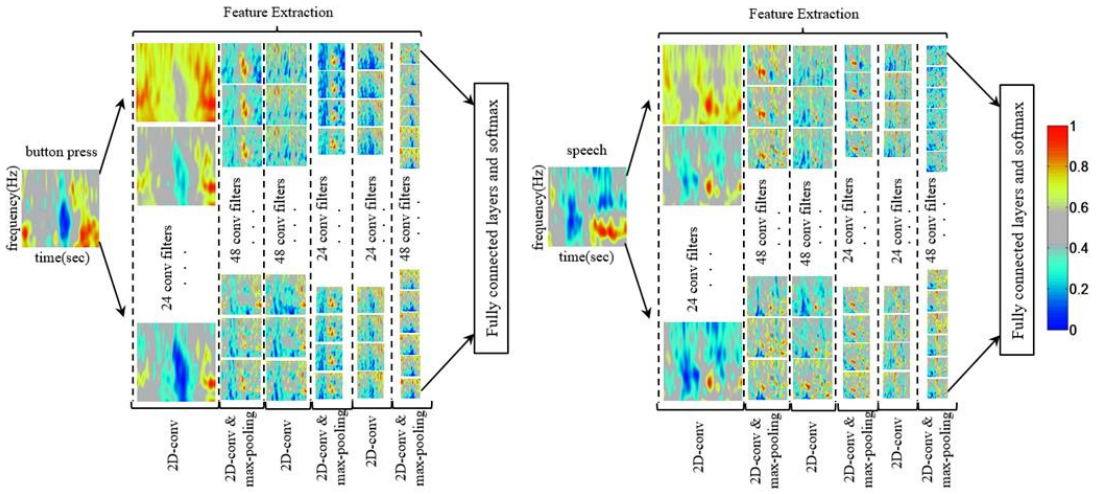

Figure 4.6. Feature maps obtained from each convolutional layer of the LFP-Net for typical behavioral tasks: Left "button press" and Right "speech". For the sake of brevity, only the feature maps of a few filters of each layer are shown here.

Table 4.3. The *p*-values obtained by comparing the proposed LFP-Net and other classifiers using Wilcoxon signed-rank test. All the classifiers were run 50 times with a randomly selected set of training, validation, and test set. Wherever the *p*-value is less than the alpha level (0.05) the difference of classification accuracy between the compared classifiers is significant, and, therefore is highlighted.

	Classifiers		
Subjects	LFP-Net vs AlexNet	LFP-Net vs Linear-SVM	LFP-Net vs RBF-SVM
1	**9.8E(-5)**	**1.6E(-5)**	**1.0E(-4)**
2	**4.7E(-4)**	**7.5E(-10)**	**7.5E(-10)**
3	7.7E(-1)	**1.4E(-9)**	**2.8E(-8)**
4	**9.7E(-3)**	**7.5E(-10)**	**7.5E(-10)**
5	**9.8E(-6)**	**7.5E(-10)**	**7.5E(-10)**
6	8.6E(-2)	**3.8E(-8)**	**5.6E(-8)**
7	**2.2E(-6)**	**2.3E(-6)**	**3.3E(-9)**
8	**8.4E(-7)**	**7.5E(-10)**	**7.5E(-10)**
9	**4.7E(-8)**	**7.5E(-10)**	**7.5E(-10)**
10	**2.6E(-7)**	**1.1E(-5)**	**4.2E(-4)**

parameters. In terms of the SVM classifier, the LFP-Net reaches a higher performance in most of the cases. For instance, in the case of subject 4, the LFP-Net significantly outperforms the RBF-SVM and Linear-SVM in 40 and 48 runs out of 50 runs respectively.

Apart from the subject-dependent analysis described above, it is worth to perform the statistical analysis in a across-subject manner. The classification accuracy of 10 subjects given in Table 4.2 is compared across different methods. Applying the Wilcoxon signed-rank test leads to the *p*-values = 0.016 when comparing the LFP-Net against the AlexNet and *p*-value = 0.006 when comparing the LFP-Net against the RBF-kernel SVM classifier.

4.3.4 LFP-Net with Different Architectures

In order to investigate how the classification performance of the proposed architecture is affected by the number of filters and convolutional layers, all experiments have been repeated by changing the network architecture.

Table 4.4. Comparing the proposed LFP-Net and other classifiers using McNemar's test. All the classifiers were run 50 times with a randomly selected set of training, validation, and test set. Since McNemar's test is calculated on a single-run basis, in each case, the number of times the calculated *p*-value < 0.05 is shown here, i.e., (#*p*-value < 0.05) / (50 runs).

	Classifiers		
Subjects	LFP-Net vs AlexNet	LFP-Net vs Linear-SVM	LFP-Net vs RBF-SVM
1	2/50	2/50	0/50
2	3/50	37/50	31/50
3	0/50	12/50	6/50
4	6/50	48/50	40/50
5	6/50	44/50	36/50
6	2/50	7/50	15/50
7	5/50	5/50	9/50
8	8/50	35/50	47/50
9	6/50	50/50	37/50
10	10/50	5/50	4/50

We observed that increasing the number of layers decreases the classification accuracy. For instance, increasing the number of convolutional layers to eight (with 24, 48, 48, 24, 24, 48, 48, 24 filters) leads to an average accuracy of ~87.5 as compared to ~88.3 given by the proposed architecture. In five subjects the classification accuracy is significantly better with the proposed architecture and in four subjects the difference is not significant.

On the other hand, decreasing the number of layers to four layers (with 24, 48, 48, 24 filters) gives an average accuracy of 87.6, while in four subjects the proposed architecture outperforms significantly and in five subjects the difference is insignificant.

Apart from the number of layers, it is worthwhile to evaluate the effect of the convolutional filters on the classification performance. In our experiments, it was observed that reducing the number of filters results in lower classification accuracy. For example, reducing the number of filters by half (12, 24, 24, 12, 12, 24) cause the average

classification accuracy falls to ~87.4; in four subjects the proposed architecture significantly surpasses, while in the rest six subjects the difference is not significant.

Increasing the number of filters imposes a considerably higher computational burden. An out-of-memory message was received from the GPU after doubling the number of filters. On the other hand, it was observed that increasing the number of filters does not lead to significantly higher performance. For instance, the average classification accuracy (88.37) slightly improved compared to the proposed architecture (88.28) when we ran the LFP-Net with 32, 55, 55, 32, 32, 55 filters. However, this difference is not significant in any of the subjects. Therefore, taking into account the computational burden and the classification performance, the proposed architecture leads to the best performance.

4.4 Summary

A deep neural network framework was presented to address the task of human behavior classification using LFP signals bilaterally recorded from STN of the brain. Decoding the brain neural response is crucial in designing the next generation of automatic brain-computer interfaces and closed-loop systems, which are aimed to adaptively interact with patients and change the therapeutic stimulation parameters based on the patients' current state.

The proposed classification method was rooted in the deep convolutional neural network architecture, which included six CNN layers, three max-pooling layers, and two fully connected layers. The softmax activation function was used at the output layer for classification of samples. Each CNN layer comprised several convolutional filters to output corresponding feature maps. The time-frequency (spectrogram) representation of the raw

STN-LFP signals within the beta frequency range (f~10-30 Hz) was used as the input to classifiers. The STN-LFPs were recorded from each bipolar re-referenced channel of the implanted DBS leads alongside the timing information ("cue" and "onset") of each trial.

Different experiments were carried out on the STN-LFPs recorded from ten subjects (provided by three separate datasets) diagnosed with Parkinson's disease (PD). Dataset1 contained the postoperative LFP recordings for two subjects recorded chronically 12 and 24 months after DBS surgery, and Datasets 2 and 3 included the intraoperative LFP recordings of eight PD subjects. For Datasets 1 and 2, three different behavioral tasks including "button press", "target-reaching", and "random segment" were considered for classification. Dataset3 also contained three classes: "button press", "speech", and "random segment". Since the neural response of each subject can be different from others, all experiments were performed in a subject-dependent manner.

The classification performance of the proposed LFP-Net was compared against other methods. The quantitative comparisons confirmed that the proposed method outperforms in most cases in terms of the classification accuracy. As such, the results of the t-test proved that the higher classification performance of the LFP-Net was significant (p-value < 0.05). As compared to AlexNet, the proposed LFP-Net architecture obtained better classification accuracy in nine out of ten subjects. It is worth mentioning that LFP-Net reached this performance with less than 2.5 million trainable variables while AlexNet required more than 31 million variables to be trained, meaning that the proposed method imposed a considerably less computational burden.

4.5 Appendix: LFP-Net with 1D Convolutional Layers

In this appendix, a different version of the LFP-Net is presented, where the 2D convolutional layers are replaced by the 1D convolutional layers. This change is done to evaluate the capability of the recorded raw LFP sequences for behavior classification as compared to its transformed time-frequency representation used throughout this chapter.

The architecture of the 1D LFP-Net is similar to figure 4.2; however, the 2D convolutional layers are replaced by the 1D layers. Moreover, the input to the network is the raw LFP signal in a time window of (-1,1)sec around each trial onset rather than the spectrogram. Note that for the convolutional layers, the time-step is set to the F_s /4, where F_s is the sampling rate of the data recording (see Table 2.1). Figure 4.7 shows the LFP-Net with 1D convolutional layers graphically.

The classification results of the 1D-conv LFP-Net is given in Table 4.5. Although using the raw LFP sequence with the 1D convolutional layers consumes much lesser computational power (i.e., it needs about 0.5 million variables to be optimized vs 2.5 million variables required for the LFP-Net architecture), the classification accuracy drops

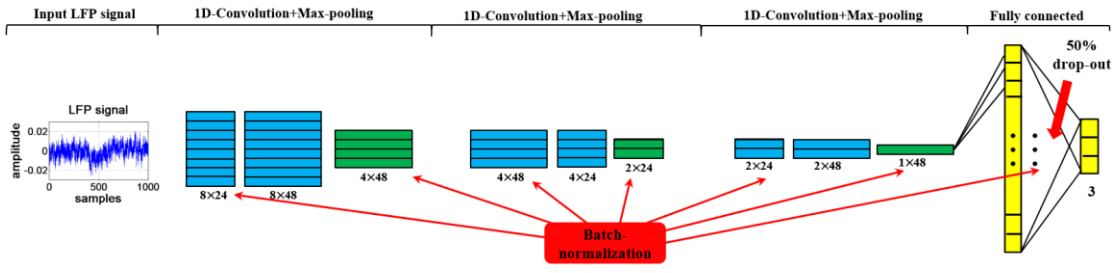

Figure 4.7. The schematic of the LFP-Net with 1D convolutional layers. The raw STN-LFP signal associated with each trial is used as the input. The network contains six convolutional+ReLU layers (blue boxes), three max-pooling layers (green boxes), and two fully connected layers (yellow box). The batch normalization (red box) is applied after each layer as shown by red arrows. The dimension of feature maps is given next to each layer.

Table 4.5. The classification accuracy (mean ± std) % of the LFP-Net with 1D convolutional layers and raw LFP sequence as input versus the original LFP-Net architecture (figure 4.3) using spectrogram as input.

	Subjects									
Classifiers	1	2	3	4	5	6	7	8	9	10
LFP-Net (1D-conv)	50.1 (2.9)	45.0 (3.3)	40.8 (4.6)	49.1 (4.1)	49.2 (3.6)	54.3 (3.7)	41.9 (5.4)	55.8 (4.5)	37.6 (5.3)	46.6 (5.3)
LFP-Net	**89.4 (2.8)**	**89.1 (2.3)**	**84.7 (3.0)**	**84.7 (3.1)**	**92.1 (2.7)**	**85.87 (3.3)**	**91.2 (2.3)**	**88.3 (3.5)**	**93.7 (2.7)**	**85.3 (4.9)**

sharply. For instance, the average accuracy of 10 subjects is about 47% when using the raw LFP sequence with 1D-conv LFP-Net. On the other hand, the average accuracy of the same 10 subjects reaches about 88% with the original LFP-Net architecture, showing the importance of using the frequency components of the LFP signals in recognizing different human activities.

4.6 Appendix: Hierarchical LFP-Net

In this section, the hierarchical classification scheme presented in Chapter 3 is extended to work with the LFP-Net as the classifier. In other words, at each level of the hierarchical structure, the LFP-Net is employed for the classification task. To evaluate the classification performance, Dataset2 is utilized. Note that, originally, Dataset2 contains 4 different tasks including "button press", "speech", "mouth movement", and "target reaching". However, for the sake of consistency with Dataset1 and Dataset3, we just did our analysis using two behavioral tasks including "button press", "target-reaching", and "random" trial, which lead to a 3-class classification problem.

In this appendix, all 4 tasks of Dataset2 plus "random" trial are included to evaluate the behavior classification using all existing behavioral tasks in Dataset2, leading to a 5-class classification problem.

The results of the single level classification is given in Table 4.6 for all subjects separately. As seen, the proposed LFP-Net obtains the best results in almost all cases. The

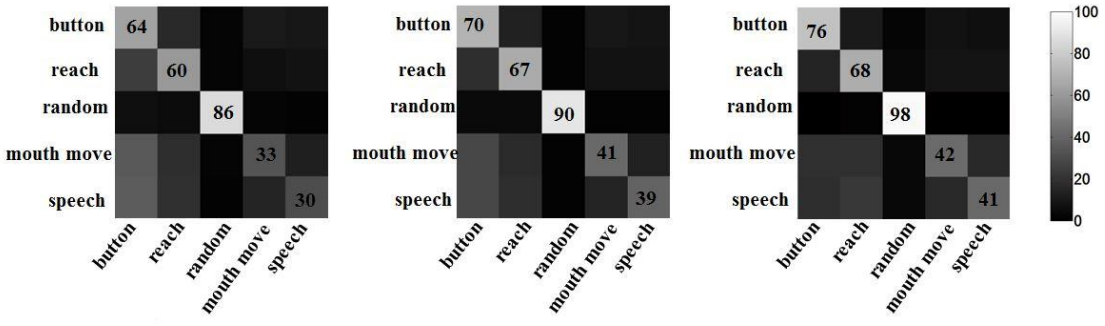

Figure 4.8. The confusion matrix of all subjects (the weighted average is shown in each case) and all behavioral tasks given for Dataset2. From left to right the results given by the SVM-RBF, SVM-Linear and the LFP-Net are given respectively.

Table 4.6. The classification accuracy (mean ± std) % of different classifiers. The results are reported for 4 subjects of Dataset2 separately. The best value is highlighted in each column across all subjects.

	Subjects			
Classifiers	1	2	3	4
LFP-Net	64.74(3.7)	**69.69(1.5)**	**73.64(2.2)**	**66.67(2.6)**
RBF-SVM	**64.86(2.8)**	62.14(3.6)	68.54(4.5)	65.94(1.6)
Linear-SVM	60.00(4.4)	51.02(5.6)	60.52(2.4)	63.07(2.4)

weighted average confusion matrix (experiments were repeated 50 times with randomly selected samples for each subject) is given in figure 4.8 for a comparison between different methods.

Apart from the single level classification for Dataset2, the hierarchical scheme has also been developed for Dataset2 with three classification levels (see chapter 3 for more details). The hierarchical scheme is shown in figure 4.9.

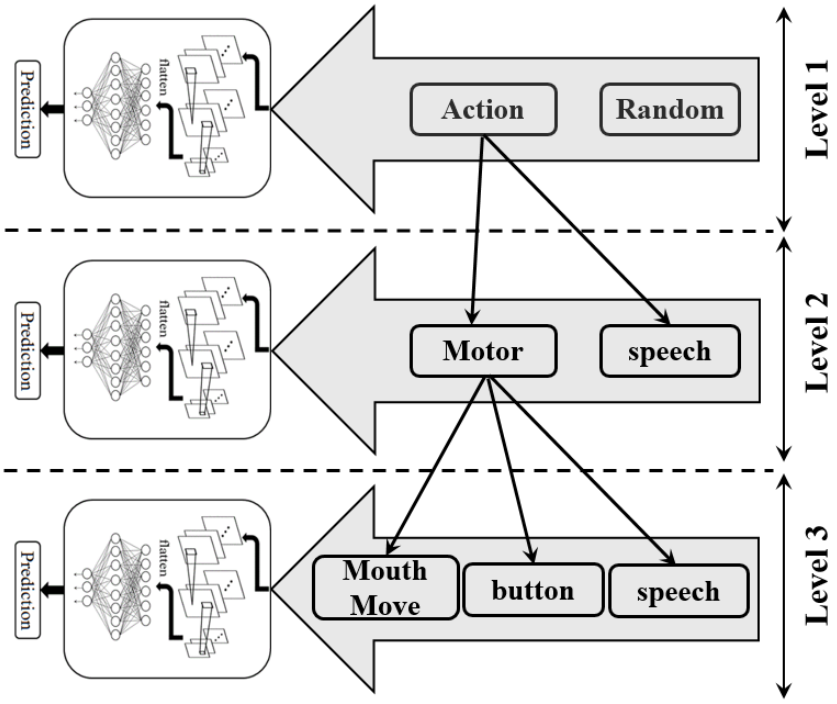

Figure 4.9. Schematic of the LFP-Net with hierarchical classification structure

Table 4.7. Classification accuracy of the LFP-Net using the hierarchical structure given in figure 4.9. The abbreviations “BP”, “MM”, “SP”, “RE”, and “RA” respectively stand for “button press”, “mouth movement”, “speech”, “reach” and “random” trials.

	subjects			
	1	2	3	4
Level 1 (Action, Random)	96.38(3.2)	95.92(2.2)	97.92(3.1)	98.76(0.25)
Level 2 (Speech, Motor, Random)	82.48(3.7)	81.53(3.3)	85.10(3.7)	83.99(2.5)
Level 3 (BP, MM, RE, SP, RA)	63.16(1.8)	64.69(4.5)	69.79(3.5)	66.45(4.0)

The classification results of the LFP-Net with hierarchical structure is given in Table 4.7 for each level of classification separately. While the LFP-Net with the hierarchical structure shows a few percent lower accuracy as compared to the single level classification (see Level 3 of Table 4.7 and Table 4.6), the hierarchical structure intrinsically has the flexibility feature. In other words, it gives the user to adjust the classification level based on the existing needs. For instance, as shown in Table 4.7, the classification accuracy is relatively high when the classification task is terminated in Level 1 or 2.

CHAPTER 5

Effects of Stimulation Pulse and Medication on Behavior Classification

This chapter presents the effects of deep brain stimulation and medication on the dynamics of brain local field potential signals used for behavior analysis of patients with Parkinson's disease. Behavior recognition from the LFP signals recorded from the subthalamic nucleus has application in developing closed-loop DBS systems, where the stimulation pulse is adaptively generated according to subjects' current behavior. Most of the existing studies on behavior recognition that use STN-LFPs are based on the DBS being "off". This chapter discovers how the performance and accuracy of automated behavior recognition from the LFP signals are affected under different paradigms of stimulation on/off. The notion of beta power suppression in LFP signals is first studied under different scenarios (stimulation on/off and medication on/off). Afterward, the accuracy of classification methods in predicting human actions using the spectrogram of STN-LFP signals is explored. Our experiments on the recorded LFP signals of two subjects confirm that the beta power is suppressed when the patients take medication or stimulation. The results also show that we can classify different behaviors with a reasonable accuracy even when the high-amplitude stimulation is applied.

5.1 Introduction

LFPs recorded from the STN are robust control signals to indicate a change in patient's Moreover, STN-LFPs correlate with symptoms of PD, levodopa medication level, behavior, and neuro-stimulation intensity [1,87]. PD symptoms may vary depending on patient's level of attention and behavior, which change the characteristics of STN-LFP activity consequently. Therefore, the chronical variability of recorded LFPs ahould be investigated to design a robust closed-loop DBS system.

To this end, we chronically recorded STN-LFP from two PD subjects in the medication on/off and stimulation on/off states while the subjects performed different motor tasks such as pressing a button and reaching a target. As a consequence, it helps explore the dynamics (i.e., change of characteristics) of LFP signals with different therapeutic conditions within a long time window. In contrast to the previous chapters, where the LFP signals were recorded in the operating room, we use a research-grade implantable neuro-stimulator (INS) to bilaterally record LFPs outside the operating room. Moreover, as opposed to our work presented in the previous chapters that utilize the LFP signals with stimulation/medication "off" condition, this study aims to evaluate the capability of human behavior recognition when stimulation/medication is "on".

First, the power spectrum density (PSD) of the recorded LFPs is analyzed to compare the effect of the medication and stimulation pulse on the increased beta power associated with PD. Then, the time-frequency representation of the raw LFP data is used for behavior classification with both stimulation/medication "off" and "on" conditions. This provides

Table 5.1. Dataset and recording details. Dataset includes several chronical recording sessions under different stimulation and medication conditions. “CH” shows the number of bipolar re-referenced LFP channels recorded for each subject. “BP” and “TR” respectively stand for “button press” and “target reaching” behavioral trials.

				Stim off & Med off		Stim off & Med on		Stim on & Med off		Stim on & Med on	
Subject	Fs(Hz)	# CH	Bandwidth (Hz)	BP	TR	BP	TR	BP	TR	BP	TR
1	422	2	0.5-100	120	120	NA	NA	120	123	120	127
2	422	2	0.5-100	120	119	120	120	60	60	120	120

valuable insight into the reliability of the classification of LFP signals in different stimulation/medication conditions.

The rest of this chapter is organized as follows: Section 5.2 elaborates on the data recording sessions. The methodology is presented in Section 5.3. The quantitative results are given in Section 5.4. Finally, Section 5.5 comprises discussion and some remarks.

5.2 Data Recording Details

Two PD subjects with an implanted DBS lead (Medtronic 3389, Minneapolis, MN, USA) in each STN and subcutaneously implanted INS (Activa^{TM} PC+S, Medtronic Inc.,) participated in this study. All participants provided informed consent in a manner approved by the HealthOne Institutional Review Board.

All subjects underwent postoperative data recording sessions. During the behavioral recording, two bipolar referenced LFPs, one from each hemisphere, were amplified and digitized (Fs ~ 422Hz) by the INS. In the experiments, the bipolar pair of channels containing the most prominent peak in beta frequency range was selected for recordings. Moreover, the INS generates a stimulation pulse with amplitude ~2.5v, frequency ~140Hz, and pulse width ~60μs.

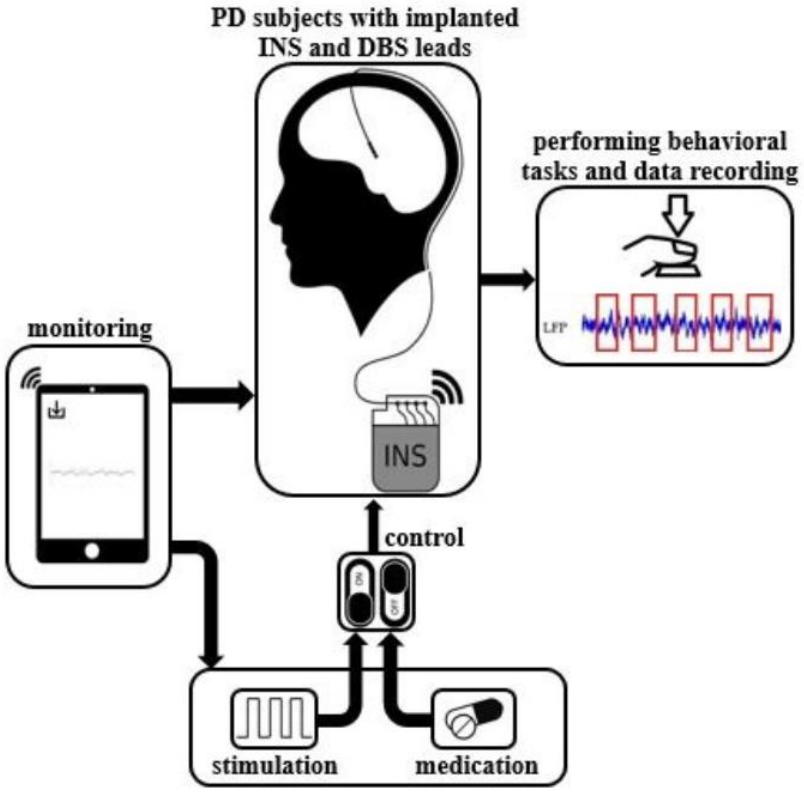

Figure 5.1. The schematic of the data recording sessions using implanted Medtronic INS system and recording setups under different medication and stimulation conditions.

Recordings were performed at 12 or 24 months after DBS lead implantation surgery. The first recording session was performed while the subjects refrained from taking their levodopa medication for at least 12 hours. The second session was performed when the subjects were regularly consuming their prescribed medication dosage. On average, behavioral tasks included 60 repetitions of cued “button press” and “target reaching” trials performed by left or right hands, under various stimulation/medication “off” and “on” conditions. The summary of the recording sessions is given in Table 5.1. Also, the schematic of the recording sessions is shown in figure 5.1.

5.3 Analysis of Stimulation and Medication Effects

In this section, first, the effect of the medication and stimulation pulse on the beta power will be presented. Then, the feature extraction and classification approach is explained.

5.3.1 Power Spectrum Density (PSD) Analysis

To compare the therapeutic effect of medication and stimulation on the increased beta power associated with PD, the power spectrum density (PSD) of the recorded LFPs are calculated using a Welch's method with a Hanning window of length nfft = F_s. This provides a frequency resolution (F_s / nfft) of 1Hz. The PSD of an LFP signal x(t) is given by its corresponding discrete Fourier transform $X(f)$ coefficients as follows [88]:

$$PSD(f) = \frac{1}{S \times F_s}|X(f)|^2, \quad S = \sum_{i=1}^{N} \omega_i^2 \tag{5.1}$$

where, S is the scaling factor defined as the sum of squared weights (ω) of the employed window (Hanning window).

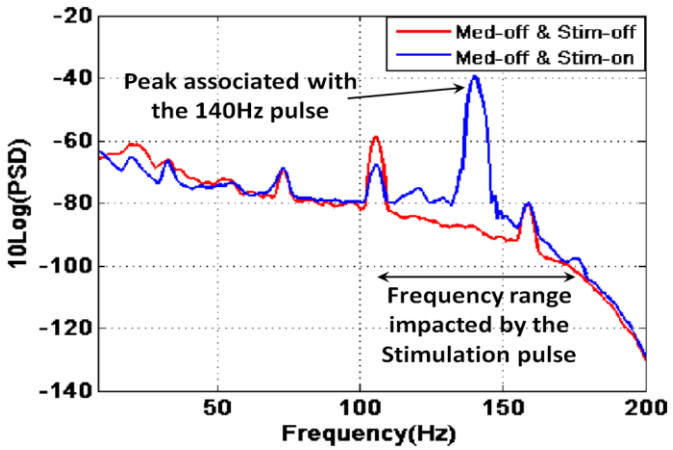

Figure 5.2. Comparison of PSDs between stimulation "off" (red) and "on" (blue) cases. As seen, the artifact imposed by the stimulation pulse mainly impacts the high frequency range f~(100-180)Hz. At the low frequency range, the beta power decreases as a result of the stimulation.

The impact of stimulation on the PSD of an exemplary LFP signal is given in figure 5.2. As shown, there is a significant peak about the stimulation frequency (f~140Hz), which has been propagated into its neighbor frequency components f~(100-180)Hz. However, the low frequency range is not considerably affected by the stimulation pulse, except for the expected therapeutic decrease on the beta power.

The effect of medication and stimulation pulse on the increased beta power of PD patients are shown in figure 5.3 and 5.4 respectively for subject 1 and 2. As can be seen,

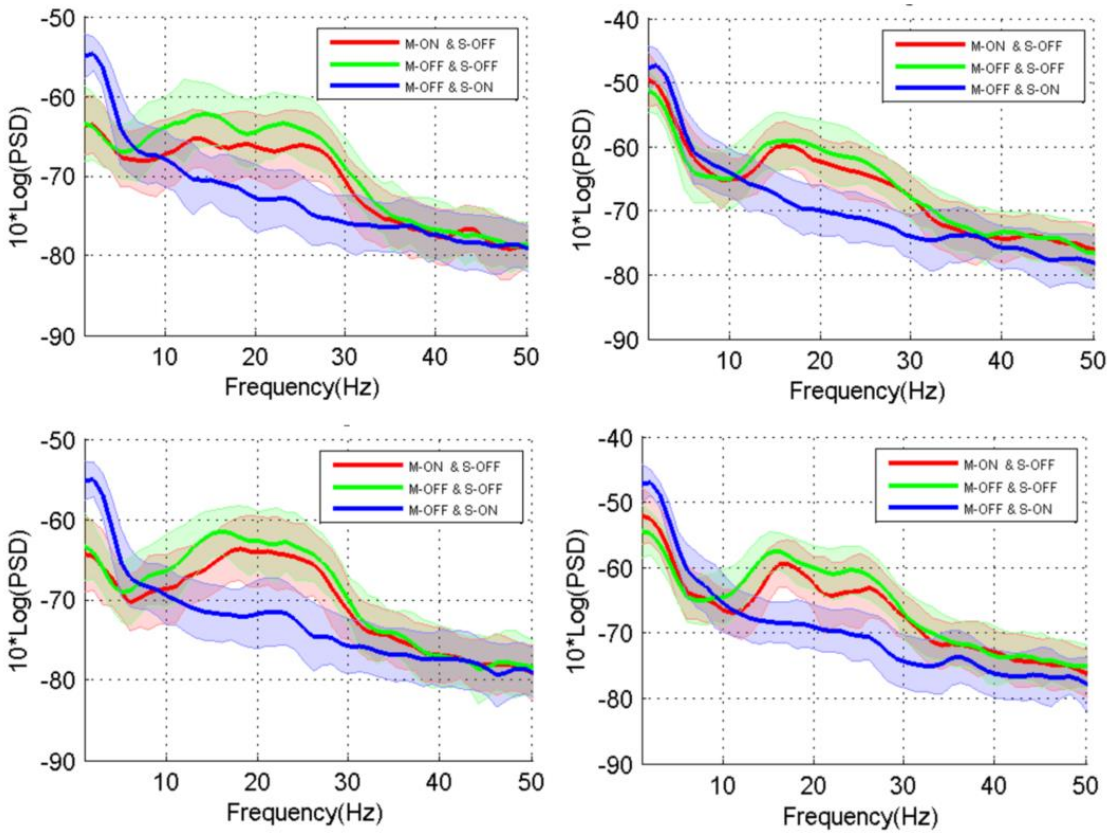

Figure 5.3. Effects of medication and stimulation pulse on the increased beta power band associated with PD for subject 1. As seen the medication or stimulation pulse tend to decrease the beta power. Top row shows the PSD of the "button press" trials and bottom row shows the PSD of "target-reaching" trial. Left and right columns respectively correspond to the LFP signal collected from left and right STNs.

the increased beta power associated with PD tends to decrease with all behavioral activities when patients take medication or therapeutic stimulation pulse.

5.3.2 Time-Frequency Analysis

As presented earlier, the time-frequency representation of the raw LFP signals is a reliable feature space to distinguish different behaviors. Intrinsically, the frequency components of the LFP signals can be impacted when a high-frequency stimulation pulse is applied. However, in Section 5.3.1, it has been shown that except for a therapeutic change

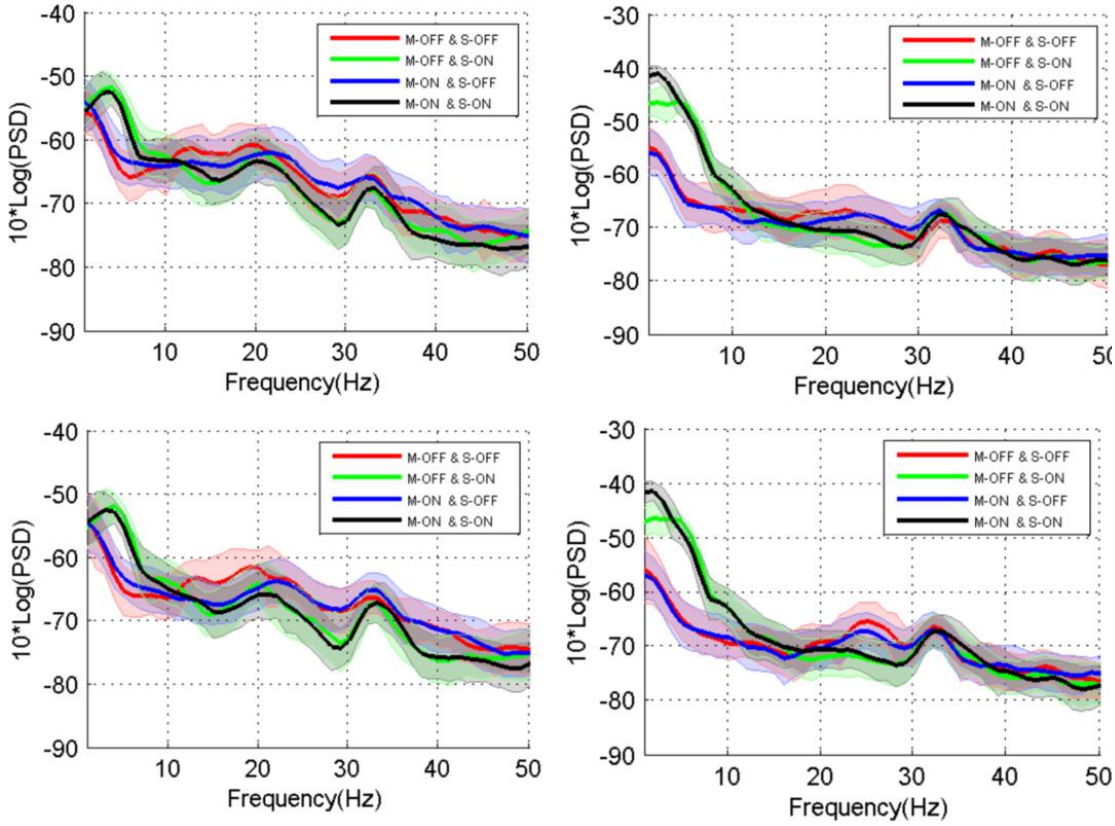

Figure 5.4. Effects of medication and stimulation pulse on the increased beta power band associated with PD for subject 2. As seen the medication or stimulation pulse tend to decrease the beta power. Top row shows the PSD of the "button press" trials and bottom row shows the PSD of "target-reaching" trial. Left and right columns respectively correspond to the LFP signal collected from left and right STNs.

in the beta power band (i.e., the increased beta power associated with PD decreases when the patients take medication or receive therapeutic stimulation), the stimulation signal mainly impacts the frequency range around the stimulation frequency (~130-185Hz).

According to our observations, except for some artifacts that appear at high-frequency components (i.e., about the stimulation frequency f~140Hz), the spectrograms obtained under stimulation off/on and medication off/on cases almost follow the same patterns within the beta frequency range. It suggests that, regardless of the stimulation or medication status, the behavior classification task can be done properly as long as the low frequency components are used. To compare the change of the beta power pattern of a typical spectrogram under different medication and stimulation conditions, figure 5.5 shows the average amplitude of the CWT coefficients of 60 trials recorded from subject 1 and "target reaching" task (Consider the similarity of the beta power band across three figures).

5.4 Experiments and Results

This section is dedicated to the classification performance under various medication and stimulation conditions using the presented LFP-Net classifier and the spectrogram as inputs.

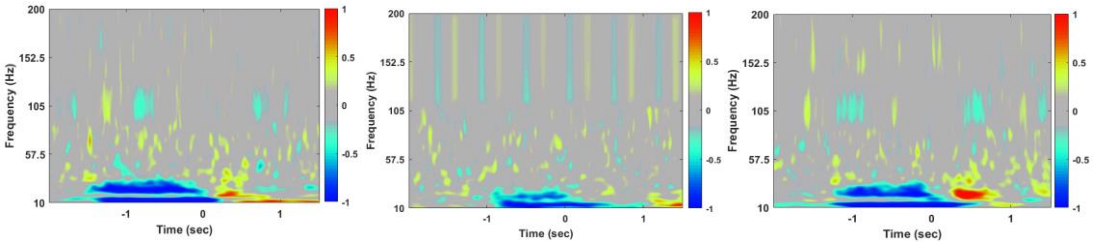

Figure 5.5. Spectrograms of different stimulation and medication conditions. Left to right respectively shows the average spectrogram of 60 "target-reaching" trials under medication "off" stimulation "off", medication "on" and stimulation "off", and medication "off" and stimulation "on" conditions. Consider the similarity of patterns within the beta frequency range (10-30Hz).

5.4.1 Classification Performance

In order to compare the behavior classification performance under different stimulation and medication conditions, the LFP-Net (chapter 4) and the recorded dataset (Table 5.1) under different conditions are employed:

1. medication “off” and stimulation “off”

2. medication “on” and stimulation “off”

3. medication “off” and stimulation “on”

The LFP-Net specifications are the same as those given in Chapter 4. A comparison between the classification performance under three aforementioned conditions is given in Table 5.2. As can be seen, the variation of the classification accuracy is not considerable under different stimulation/medication status, confirming that the time-frequency representation within the beta frequency band is still a reliable candidate for classification task regardless of the stimulation/medication status. For instance, while subject 2 shows less than 3% drop on the average accuracy with stimulation “on” condition, subject 1 obtains more the 3% improvement on the average classification accuracy under stimulation “on” condition.

Table 5.2. The classification accuracy (mean ± std) % of the proposed LFP-Net under different stimulation and medication condition for Dataset-I (i.e., subject 1 and 2). The average and standard deviation of 50 repetitions is given in each case.

	medication and stimulation condition		
Subjects	stimulation off medication off	stimulation off medication on	stimulation on medication off
1	89.4(2.8)	92.1(4.0)	93.7(1.7)
2	89.1(2.3)	88.3(3.3)	86.3(3.6)

5.4.2 Statistical Analysis

In order to statistically compare the classification performance under different medication and stimulation conditions, the McNemar's test (see Section 2.5) is used. As a result, 50 *p*-values are obtained for 50 runs for each medication/stimulation conditions associated with Table 5.2. The number of *p*-value < 0.05 over 50 runs for each case is given in Table 5.3. As can be seen, based on the McNemar's test, the classification power of the LFP-Net is not significantly different based on different medication/stimulation conditions, which can emphasize that the beta frequency range can still be a reliable candidate for behavior classification even if the patients take medication or therapeutic stimulation pulse.

5.5 Summary

In this chapter, the effect of the stimulation pulse and medication on the human behavior classification and beta power of Parkinson's disease patients was evaluated. A feature space based on the time-frequency representation of the acquired brain subthalamic nucleus local field potential signals was developed. Our analysis showed that the beta frequency components of LFPs are capable of detecting different human activities even when the high-amplitude deep brain stimulation pulse is applied.

Table 5.3. Comparing the classification performance of the proposed LFP-Net with different medication/stimulation conditions and McNemar's statistical test. All the classifiers were run 50 times with a randomly selected set of training, validation, and test set. Since McNemar's test is calculated on a single-run basis, in each case, the number of times the calculated *p*-value < 0.05 is shown here, i.e., (#*p*-value < 0.05) / (50 runs).

Subjects	(stim off, med off) vs (stim off, med on)	(stim off, med off) vs (stim on, med off)
1	7/50	17/50
2	2/50	10/50

Different experiments were carried out on the LFP signals acquired from two PD subjects to classify “button press”, “target reaching” and “random” trials. The performance of behavior classification was evaluated under stimulation/medication “off” and “on” conditions. The results showed that, regardless of the stimulation/medication status, the behavior classification capability remains almost unchanged when the beta frequency components of the proposed feature space are used. As a result, there is no need to remove the high-frequency artifacts imposed by the stimulation pulse, which essentially requires more computational power.

Furthermore, the effect of stimulation and medication on the beta power of LFP signal was separately investigated. The results showed that the stimulation artifact mainly impacts the frequency range around the stimulation frequency. Also, the increased beta power associated with PD is suppressed significantly when the patients take medication or receive therapeutic stimulation.

CHAPTER 6

Conclusion and Future Directions

6.1 Conclusion and Discussion

Neuro-stimulation is a neurosurgical procedure that modifies the brain's electrical activity to provide potential treatments for a large spectrum of neurological disorders, such as Parkinson's disease (PD), essential tremor, depression, seizures, and chronic pain. Neuro-stimulation modulates local field potential oscillations in the deep brain nuclei and affects cortical and subcortical connections, key to decision-making, learning and cognitive association. Considering the effectiveness of brain electrical stimulation techniques in elevating patients' symptoms, they have gained much attention in recent years, leading to designing more advanced implantable electrical stimulator devices and brain surgery techniques.

In particular, deep brain stimulation (DBS) is a rapidly growing technique in neuroscience community, and is highly used when drug therapy in no longer effective for patients. DBS is an FDA-approved therapy for essential tremor and Parkinson's disease, and provides significant benefit over medical therapy. Candidacy for DBS is typically determined by balancing the potential quality of life gains from DBS with the potential

clinical risks of DBS implantation. Although DBS provides substantial relief of the motor signs of PD, it has negative side effects. An empirical question remains regarding the effectiveness of the DBS approach caused by lack of additivity and optimality. An adaptive DBS system could provide unique parameters for disparate behavior, providing superior therapeutic benefit for the task at the moment, without the cost of compromising performance for tasks performed later. Furthermore, an adaptive system may also reduce power consumption by only turning on the pulse generator when needed. Recognition of human behavior through neural feedbacks from the brain is a stepping-stone for designing a closed-loop DBS system that can adaptively change the parameters of the stimulation signals based on patients' current condition.

This dissertation was mainly concentrated on the recognition of human behavioral activities through the recorded local field potential (LFP) signals from subthalamical nucleus (STN) of PD patients. Note that DBS provides a unique opportunity to record *in vivo* the neural responses through acquiring LFP signals, allowing the investigation of electrical oscillatory activities of the brain. Specifically, LFPs recorded from the STN are robust control signals indicating a change in the patients' state, correlating with the patients' PD symptoms, medication level, and behavior. Furthermore, LFP signals are stable over long periods, which is a necessary characteristic for a feedback signal in a closed-loop DBS system.

The time-frequency representation of the LFP signal within the beta range (~10-30 Hz) is used as feature space to classify behavioral activities. It was observed beta power desynchronization during activities followed by an augmentation in majority of subjects'

STN-LFP recordings. Several classifiers were developed to classify different human behavioral tasks including, button press, target reaching, mouth movement, and speech.

A hierarchical structure was proposed to perform the behavior classification via a multi-level framework, which is able to recognize human behavior at different levels of resolution ranging from a coarser level, like action recognition to a finer level, like finger movement. An Lp-norm MKL-based SVM classifier was trained for behavior classification task at each level of the proposed hierarchical approach. All bipolar LFP signals recorded from both STNs were combined via the MKL formulation to recognize the label of the corresponding trial. To reduce computational costs, a feature selection method was alternatively developed that still incorporated all recorded LFP data using a pairwise strategy. An FFT-based phase synchronization approach was used to form three interhemispheric pairs out of six available bipolar LFP signals. Three classifiers were then driven at the same time, leading to three labels for the corresponding trial. Finally, these labels were passed through a fusion function to determine a single label for the input trial.

One of the limitations of this work is that it was developed based on the existence of all six recorded bipolar STN-LFPs. Although this is feasible in the research environment, in practice, only a few of the contacts of the DBS leads (1 or 2 bipolar re-referenced contacts) are is used for recording based on the location of the lead and the strength of the signals sensed from the lead contacts.

To address this limitation, presented LFP-Net was presented, which is a deep neural network framework for human behavior classification using a single bipolar re-referenced LFP signal recorded from either STNs. The proposed classification method was rooted on

the deep convolutional neural network architecture, which was composed of six CNN layers, three max-pooling layers, and two fully connected layers. The softmax activation function was used at the output layer for classification of samples.

Different experiments were carried out on the STN-LFPs recorded from ten subjects diagnosed with Parkinson's disease (PD). The classification performance of the proposed classification methods were compared against other methods. The quantitative comparisons confirmed that the proposed methods improve the behavior recognition performance in most cases. Specifically, the deep learning classifier showed much higher potentials in human behavior recognition using LFP signals as compared to the traditional classification approaches (e.g., SVM, KNN, etc) presented in related literature.

The effect of the stimulation pulse and medication on the human behavior classification and beta power of PD patients were also studied. Our analysis showed that the beta frequency components of LFPs are capable of detecting different human activities even when the high-amplitude deep brain stimulation pulse is applied. The performance of behavior classification was evaluated under different stimulation/medication "off/on" conditions. The results showed that, regardless of the stimulation/medication status, the behavior classification capability remains almost unchanged when the beta frequency components are used as feature space. As a consequence, there is no need to remove the high-frequency artifacts imposed by the stimulation pulse, which essentially requires more computational power. Furthermore, the effect of stimulation and medication on the beta power of LFP signal was separately investigated. The results showed that the stimulation artifact mainly impacts the frequency range around the stimulation frequency. Also, the

increased beta power associated with PD is suppressed significantly when the patients take medication or receive therapeutic stimulation.

6.2 Future Work

Intelligent closed-loop systems and brain computer interfaces are fast growing areas in neuroscience research community and industry. Some of the future research outlines and interesting extensions to this work are as follows:

- Throughout this work the recorded timing information during data collection sessions was used to identify the segments of the LFP signals related to each task. However, for a behavior-adapted closed-loop system, this timing information needs to be detected automatically. So, one interesting extension to this work is to develop event-related biomarkers, which will be able to automatically detect the event-modulated clues, pinpointing the initiation of each event accordingly.
- A crucial part of designing an adaptive closed-loop system is to adjust the parameters of the stimulation signal such as pulse width, stimulation frequency, and amplitude based on the patients' current behavior. So, another future direction of this work will be finding the optimum DBS parameters for different behaviors and investigate the capability of the pulse generator for changing the stimulation parameters automatically.
- Throughout this research, we used LFP signals as the only brain feedback to identify different behavioral activities. Even though we achieved promising results, to obtain a perfect classification performance, the information provided

by the LFP signals may not be sufficient. So, investigating the feasibility of incorporating the other bio-signals such as ECG, EMG, and ECoG alongside the LFP signal to obtain a higher behavior recognition performance would be another interesting future work.

- Investigating the power consumption and computational capability of the implantable pulse generator is another key future research direction. Although the training part of classification algorithms and other required processing steps can be done offline, it is important to assess how the computational complexity of algorithms can be conducted for online applications and how the battery lifetime will be affected by continuous recording of the neural response.
- Apart from the adaptive closed-loop DBS systems, the results of this work can be used for other brain computer interface (BCI) applications, behavior recognition based on other brain signals such as EEG and ECoG, and related animal studies.

Bibliography

[1] A. O. Hebb, F. Darvas, and K. J. Miller, "Transient and state modulation of beta power in human subthalamic nucleus during speech production and finger movement," Neuroscience., vol. 202, pp. 218-233, 2012.

[2] F. Darvas, and A. O. Hebb, "Task specific inter-hemispheric coupling in human subthalamic nuclei," Frontiers in Human Neuroscience., vol. 8, Article 701, Sep. 2014.

[3] J. Zhuang, W. Truccolo, C. Varagas-Irwin, and J. P. Donoghue, "Decoding 3-Dreach and grasp kinematics from high-frequency local field potentials in primate primary motor cortex," IEEE Trans. Biomed. Eng., vol. 57, no. 7, pp. 1774–1784, 2010.

[4] K. A. Follett, F. M. Weaver, M. Stern, K. Hur, C. L. Harris, P. Luo, W. J. Marks, J. Rothlind, O. Sagher, C. Moy, and R. Pahwa, "Pallidal versus subthalamic deep-brain stimulation for Parkinson's disease," N. Engl. J. Med., vol. 362, pp. 2077–2091, 2010.

[5] A. Abosch, D. Lanctin, I. Onaran, L. Eberly, M. Spaniol, and N. F. Ince, "Long-term recordings of local field potentials from implanted deep brain stimulation electrodes," Neurosurgery, vol. 71, pp. 804–814, 2012.

[6] G. Giannicola, M. Rosa, D. Servello, C. Menghetti, G. Carrabba, C. Pacchetti, R. Zangaglia, F. Cogiamanian, E. Scelzo, and S. Marceglia, "Subthalamic local field potentials after seven-year deep brain stimulation in Parkinson's disease," Exp. Neurol., vol. 237, no. 2, pp. 312–317, 2012.

[7] T. Foltynie, L. Zrinzo, I. Martinez-Torres, E. Tripoliti, E. Petersen, E. Holl, I. Aviles-Olmos, M. Jahanshahi, M. Hariz, and P. Limousin, "MRI-guided STN DBS in Parkinson's disease without microelectrode recording: efficacy and safety," Journal of Neurology, Neurosurgery & Psychiatry, vol. 82, no. 4, pp. 358-363, 2011.

[8] J. Y. Lee, J. W. Kim, J-Y. Lee, Y. H. Lim, C. Kim, D. G. Kim, B. S. Jeon, and S. H. Paek, "Is MRI a reliable tool to locate the electrode after deep brain stimulation surgery? comparison study of CT and MRI for the localization of electrodes after DBS," Acta neurochirurgica, vol. 152, no. 12, pp. 2029-2036, 2010.

[9] M. I. Hariz, "Complications of deep brain stimulation surgery," Movement disorders, vol. 17, no. 3, pp. 162-166, 2002.

[10] J-H. Heo, K-M. Lee, S. H.Paek, M-J. Kim, J-Y. Lee, J-Y. Kim, S-Y. Cho, Y. H. Lim, M-R. Kim, S. Y. Jeong, "The effects of bilateral subthalamic nucleus deep brain stimulation (STN DBS) on cognition in Parkinson's disease," Journal of the neurological sciences, vol. 273, no. 1, pp. 19-24, 2008.

[11] A. Abosch, D. Lanctin, I. Onaran, L. Eberly, M. Spaniol, and N. F. Ince, "Long-term recordings of local field potentials from implanted deep brain stimulation electrodes," Neurosurgery., vol. 71, no. 4, pp. 804–814. 2012.

[12] B. Rosin, M. Slovik, R. Mitelman, M. Rivlin-Etzion, S. N. Haber, Z. Israel, E. Vaadia, and H. Bergman, "Closed-loop deep brain stimulation is superior in ameliorating Parkinsonism," Neuron., vol. 72, pp. 370–384, 2011.

[13] S. Santaniello, G. Fiengo, L. Glielmo, and W. M. Grill, "Closed-loop control of deep brain stimulation: a simulation study," IEEE Trans. Neural Syst. Reh Eng., vol. 19, no. 1, pp. 15–24, 2011.

[14] S. Little, A. Pogosyan, S. Neal, B. Zavala, L. Zrinzo, M. Hariz, T. Foltynie, P. Limousin, K. Ashkan, and J. FitzGerald, "Adaptive deep brain stimulation in advanced Parkinson disease," Ann. Neurol., vol. 74, no. 3, pp. 449–457, 2013.

[15] K. J. Friston, A. M. Bastos, D. Pinotsis, and V. Litvak, "LFP and oscillations-what do they tell us?" Curr. Opin. Neurobiol., vol. 31, pp. 1–6, 2015.

[16] S. Little, and P. Brown, "What brain signals are suitable for feedback control of deep brain stimulation in Parkinson's disease?," Ann. N. Y. Acad. Sci., vol. 1265, pp. 9–24, 2012.

[17] D. Williams, M. Tijssen, G. Van Bruggen, A. Bosch, A. Insola, V. Di Lazzaro, P. Mazzone, A. Oliviero, A. Quartarone, and H. Speelman, "Dopamine-dependent changes in the functional connectivity between basal ganglia and cerebral cortex in humans," Brain J. Neurol., vol. 125, pp. 1558–1569, 2002.

[18] C. Loukas, and P. Brown, "Online prediction of self-paced hand-movements from subthalamic activity using neural networks in Parkinson's disease," J. Neurosci. Methods., vol. 137, pp. 193–205, 2004.

[19] R. D. Flint, Z. A. Wright, M. R. Scheid, and M. W. Slutzky, "Long term, stable brain machine interface performance using local field potentials and multiunit spikes," J. Neural Eng., vol. 10, 2013.

[20] B. Blankertz, S. Lemm, M. Treder, S. Haufe, and K.-R. Müller, "Single-trial analysis and classification of ERP components—a tutorial," Neuroimage., vol. 56, no. 2, pp. 814–825, 2011.

[21] F. Lotte, M. Congedo, A. Lécuyer, F. Lamarche, and B. Arnaldi, "A review of classification algorithms for EEG-based brain–computer interfaces," J. Neural Eng, vol. 4, no. 2, pp. 1–13, 2007.

[22] H. Sheikh, D. J. McFarland, W. A. Sarnacki, and J. R. Wolpaw, "Electroencephalographic (EEG)-based communication: EEG control versus system performance in humans," Neurosci. Lett., vol. 345, no. 2, pp. 89–92, 2003.

[23] J. R. Millán, F. Renkens, J. Mourino, and W. Gerstner, "Non-invasive brain-actuated control of a mobile robot by human EEG," IEEE Trans. Biomed. Eng., vol. 51, no. 6, pp. 1026–1033, 2004.

[24] J. R. Wolpaw, N. Birbaumer, D. J. McFarland, G. Pfurtscheller, and T. M. Vaughan, "Brain-computer interfaces for communication and control," Clin. Neurophysiol., vol. 113, pp. 767–791, 2002.

[25] M. S. Treder, B. Blankertz, "overt attention and visual speller design in an ERP-based brain-computer interface," Behav. Brain Funct., vol. 6, no. 28, 2010.

[26] V. Bostanov, “BCI competition 2003-data sets Ib and IIb: feature extraction from event-related brain potentials with the continuous wavelet transform and the t-value scalogram,” IEEE Trans. Biomed. Eng., vol. 51, no. 6, pp. 1057–1061, 2004.

[27] M. Kaper, P. Meinicke, U. Grossekathoefer, T. Lingner, H. Ritter, “BCIcompetition 2003—data set IIb: support vector machines for the P300 speller paradigm,” IEEE Trans. Biomed. Eng., vol. 51, no. 6, pp. 1073–1076, 2004.

[28] Y. Li, C. Guan, H. Li, Z. Chin, "A self-training semi-supervised SVM algorithm and its application in an EEG-based brain computer interface speller system," Pattern Recognit. Lett., vol. 29, no. 9, pp. 1285–1294, 2008.

[29] G. Dornhege, B. Blankertz, G. Curio, K. R. Müller, “Combining features for BCI,” Proc. Adv. Neural Inf. Process. Syst. vol. 15, pp. 1115–1122, 2003.

[30] G. Dornhege, B. Blankertz, G. Curio, K. R. Müller, “Increase information transfer rates in BCI by CSP extension to multi-class,” Proc. Adv. Neural Inf. Process. Syst. vol. 16, pp. 773–740, 2004.

[31] G. Blanchard, B. Blankertz, “BCI competition 2003—Data set IIa: spatial patterns of self-controlled brain rhythm modulations,” IEEE Trans. Biomed. Eng., vol. 51, no. 6, pp. 1062–1066, 2004.

[32] R. Scherer, G. Muller, C. Neuper, B. Graimann, G. Pfurtscheller, “An asynchronously controlled EEG-based virtual keyboard: improvement of the spelling rate,” IEEE Trans. Biomed. Eng., vol. 51, no. 6, pp. 979–984, 2004.

[33] R. C. Panicker, S. Puthusserypady, Y. Sun, “An asynchronous p300 BCI with SSVEP-based control state detection,” IEEE Trans. Biomed Eng., vol. 58, no. 6, pp. 1781–1788, 2011.

[34] G. R. Muller-Putz, V. Kaiser, T. Solis-Escalante, G. Pfurtscheller, “Fast set-up asynchronous brain-switch based on detection of foot motor imagery in1-channel EEG,” Med. Biol. Eng. Comput., vol. 48, no. 3, pp. 229–233, 2010.

[35] X. An, D. Kuang, X. Guo, Y. Zhao, and L. He, “A deep learning method for classification of EEG data based on motor imagery,” Intelligent Computing in Bioinformatics., pp. 203–210, 2014.

[36] D . Wulsin, J. Gupta, R. Mani, J. Blanco, and B. Litt, “Modeling electroencephalography waveforms with semi supervised deep belief nets: fast classification and anomaly measurement,” J. Neural Eng., vol. 8, no. 3, 2011.

[37] H. Yang, S. Sakhavi, K. K. Ang, and C. Guan, “On the use of convolutional neural networks and augmented CSP features for multi-class motor imagery of EEG signals classification,” Engineering in Medicine and Biology Society (EMBC), 37th IEEE International Conference on., pp 2620–2623, 2015.

[38] Y. Rezaei Tabar, and H. Ugur, “A novel deep learning approach for classification of EEG motor imagery signals,” Journal of Neural Eng., vol. 14, no. 1, 2016.

[39] S. Niketeghad, A. O. Hebb, J. Nedrud, S. J. Hanrahan, and M. H. Mahoor, “Motor task event detection using subthalamic nucleus local field potentials,” Engineering in Medicine and Biology Society (EMBC), 37th IEEE International Conference on., pp. 5553–5556, 2015.

[40] H. M. Golshan, A. O. Hebb, S. Hanrahan, J. Nedrud, and Mohammad H. Mahoor, "A multiple kernel learning approach for human behavioral task classification using STN-LFP signal," Engineering in Medicine and Biology Society (EMBC), 38th IEEE International Conference on., 2016.

[41] H. M. Golshan, A. O. Hebb, S. J. Hanrahan, J. Nedrud, and M. H. Mahoor, "An FFT-based synchronization approach to recognize human behaviors using STN-LFP signal," ICASSP, 42nd IEEE International Conference on., pp. 979-983, 2017.

[42] H. M. Golshan, A. O. Hebb, S. J. Hanrahan, J. Nedrud, and M. H. Mahoor, "A hierarchical structure for human behavior classification using STN local field potentials," Journal of Neuroscience Methods., vol. 293, pp. 254-263, 2018.

[43] H. M. Golshan, A. O. Hebb, J. Nedrud, and M. H. Mahoor, "Studying the Effects of Deep Brain Stimulation and Medication on the Dynamics of STN-LFP Signals for Human Behavior Analysis," Engineering in Medicine and Biology Society (EMBC), 40th IEEE International Conference on., pp. 4720-4723, 2018.

[44] N. Zaker, A. Dutta, A. Maurer, J. J. Zhang, S. J. Hanrahan, A. O. Hebb, and N. Kovvali, "Adaptive Learning of Behavioral Tasks for Patients with Parkinson's Disease Using Signals from Deep Brain Stimulation," Signals, Systems and Computers, Asilomar Conference on., pp. 208-212, 2014.

[45] S. Niketeghad, A. O. Hebb, J. Nedrud, S. J. Hanrahan , and M. H. Mahoor, "Motor Task Detection From Human STN Using Interhemispheric Connectivity," IEEE Trans. Neural Syst. Reh. Eng., vol. 26, no. 1, 2018.

[46] J.A. Obeso, M.C. Rodriguez-Oroz, B. Benitez-Temino, F.J. Blesa, J. Guridi, C. Marin, and M. Rodriguez, "Functional organization of the basal ganglia: therapeutic implications for Parkinson's disease.", Mov Disord., vol. 23, pp. 548-559, 2008.

[47] A. O Hebb, J. J. Zhang, M. H. Mahoor, C. Tsiokos, C. Matlack, H. J. Chizeck, and N. Pouratian, "Creating the feedback loop: closed-loop neurostimulation," Neurosurgery Clinics of North America., vol. 25, no. 1, pp. 187-204, 2014.

[48] G. Foffani, A.M. Bianchi, G. Baselli, and A. Priori, "Movement-related frequency modulation of beta oscillatory activity in the human subthalamic nucleus," Journal of Physiology., vol 568, no. 2, pp.699-711, 2005.

[49] A. A. Kuhn, D. Williams, A. Kupsch, P. Limousin, M. Hariz, G-H. Schneider, K. Yarrow, and P. Brown, "Event-related beta desynchronization in human subthalamic nucleus corrolates with motor performance," Brain., vol. 127, no. 4, pp.735-746, 2004.

[50] B. J. Bordini, A. Garg, C. L. Gallagher, B. Bell, and P. C. Garell, "Neuropsychological effects of bilateral deep brain stimulation of the subthalamic nucleus in Parkinson's disease," Stereotact. Funct. Neurosurg., vol. 85, pp. 113–120, 2007.

[51] E. Tripoliti, L. Zrinzo, I. Martinez-Torres, E. Frost, S. Pinto, T. Foltynie, E. Holl, E. Petersen, M. Roughton, and M. I. Hariz, "Effects of subthalamic stimulation on speech of consecutive patients with Parkinson disease," Neurology, vol. 76, pp. 80–86, 2011.

[52] F. J. Santos, R. M. Costa, and F. Tecuapetla, “Stimulation on demand: closing the loop on deep brain stimulation,” Neuron., vol. 72, no. 2, pp. 197-198, 2011.

[53] V. Fleury, P. Pollak, J. Gere, G. Tommasi, L. Romito, C. Combescure, E. Bardinet, S. Chabardes, S. Momjian, and A. Krainik, “Subthalamic stimulation may inhibit the beneficial effects of levodopa on akinesia and gait,” Mov. Disord., vol. 31, pp. 1389–1397, 2016.

[54] M. Arlotti, L. Rossi, M. Rosa, S. Marceglia, and A. Priori, “An external portable device for adaptive deep brain stimulation (aDBS) clinical research in advanced Parkinson’s disease,” Med. Eng. Phys., vol. 38, pp. 498–505, 2016.

[55] P. Mahlknecht, P. Limousin, and T. Foltynie, “Deep brain stimulation for movement disorders: Update on recent discoveries and outlook on future developments,” J. Neurol., vol. 262, pp. 2583–2595, 2015.

[56] A.O. Hebb, J. J. Zhang, M. H. Mahoor, C. Tsiokos, C. Matlack, H. J. Chizeck, and N. Pouratian, “Creating the Feedback Loop,” Neurosurg. Clin. N. Am., vol. 25, pp. 187–204, 2014.

[57] G. Deuschl, J. Herzog, G. Kleiner-Fisman, C. Kubu, A. M. Lozano, K. E. Lyons, M. C. Rodriguez-Oroz, F. Tamma, A. I. Troster, and J. L. Vitek, “Deep brain stimulation: postoperative issues,” Mov. Disord., vol. 21, pp. 219–237, 2006.

[58] C. Hammond, H. Bergman, and P. Brown, “Pathological synchronization in Parkinson’s disease: networks, models and treatments,” Trends Neurosci., vol. 30, pp. 357–364, 2007.

[59] J. Y. Lee, B. S. Jeon, S. H. Paek, Y. H. Lim, M. R. Kim, and C. Kim, “Reprogramming guided by the fused images of MRI and CT in subthalamic nucleus stimulation in Parkinson disease,” Clin. Neurol. Neurosurg., vol. 112, pp. 47–53, 2010.

[60] S. Stanslaski, P. Afshar, P. Cong, J. Giftakis, P. Stypulkowski, D. Carlson, D. Linde, D. Ullestad, A.-T. Avestruz, and T. Denison, “Design and validation of a fully implantable, chronic, closed-loop neuromodulation device with concurrent sensing and stimulation,” IEEE Trans. Neural Syst. Rehabil. Eng., vol. 20, pp. 410–421, 2012.

[61] J. Li, L. Zhang, D. Tao, H. Sun, and Q. Zhao, “A prior Neurologistic knowledge free tensor-based scheme for single trial EEG classification,” IEEE Trans. Neural Syst. Reh. Eng., vol. 17, no. 2, pp. 107-115, Apr. 2009.

[62] F. Darvas, and A. O. Hebb, “Task specific inter-hemispheric coupling in human subthalamic nuclei,” Frontiers in Human Neuroscience., vol. 8, Article 701, Sep. 2014.

[63] I. T. Jolliffe, “Principal Component Analysis,” New York, NY, USA: Springer-Verlag, 1986.

[64] X. Zhang, M. H. Mahoor, and S. M. Mavadati, “Facial expression recognition using lp-norm MKL multiclass-SVM,” Machine Vision and Applications., vol. 26, pp. 467-482, Apr. 2015.

[65] M. Kloft, U. Brefeld, U. Sonnenburg, and A. Zien, “Lp-norm multiple kernel learning,” J. Mach. Learn. Res., vol. 12, pp. 953-997, 2011.

[66] S. Sonnenburg, G. Rätsch, C. Schäfer, and B. Schölkopf, “Large scale multiple kernel learning,” J. Mach. Learn. Res., vol. 7, pp. 1531–1565, 2006.

[67] A. Rakotomamonjy, F. Bach, S. Canu, and Y. Grandvalet, “SimpleMKL,” J. Mach. Learn. Res., vol. 9, pp. 2491–2521, 2008.

[68] M. Gönen, and E. Alpaydin, “Multiple kernel learning algorithms,” J. Mach. Learn. Res., vol. 12, pp. 2211–2268, 2011.

[69] A. Krizhevsky, I. Sutskever, and G. E. Hinton, “Imagenet classification with deep convolutional neural networks,” Advances in neural information processing systems, pages1097–1105, 2012.

[70] D, Jia, W. Dong, R. Socher, L-J Li, K. Li, and L. Fei-Fei, “Imagenet: A large-scale hierarchical image database,” CVPR, IEEE conference on., pp. 248-255, 2009.

[71] H. Rezaeilouyeh, A. Mollahosseini, and Mohammad H. Mahoor, “Microscopic medical image classification framework via deep learning and shearlet transform,” Journal of Medical Imaging., vol. 3, no. 4, pp. , 2016.

[72] R. Hecht-Nielsen, “Theory of the backpropagation neural network,” Neural networks for perception., pp. 65-93, 1992.

[73] J. Demšar, “Statistical comparisons of classifiers over multiple data sets,” Journal of Machine learning research., vol. 7, pp. 1-30, 2006.

[74] F. Aboitiz, J. López, and J. Montiel, “Long distance communication in the human brain: timing constraints for inter-hemispheric synchrony and the origin of brain lateralization,” Biological research, vol. 36, no. 1, pp. 89-99, 2003.

[75] Kajal, D. Singh, C. Braun, J. Mellinger, M. D. Sacchet, S. Ruiz, E. Fetz, N. Birbaumer, and R. Sitaram, “Learned control of inter-hemispheric connectivity: Effects on bimanual motor performance,” Human brain mapping., vol. 38, no. 9, pp. 4353-4369, 2017.

[76] S. Ovadia-Caro, Y. Nir, A. Soddu, M. Ramot, G. Hesselmann, A. Vanhaudenhuyse, and S. Laureys, “Reduction in inter-hemispheric connectivity in disorders of consciousness,” PLoS One, vol. 7, no. 5, 2012.

[77] K. A. Mamun, M. Mace, M. E. Lutman, J. Stein, X. Liu, T. Aziz, R. Vaidyanathan, and S. Wang, “Movement decoding using neural synchronization and inter-hemispheric connectivity from deep brain local field potentials,” J. Neural Eng., vol. 12, Aug. 2015.

[78] S. Little, H. Tan, A. Anzak, A. Pogosyan, A. Kuhn, and P. Brown, “Bilateral Functional Connectivity of the Basal Ganglia in Patients with Parkinson’s Disease and Its Modulation by Dopaminergic Treatment,” PLoS ONE., vol. 8, no. 12, 2013.

[79] K. Majumdar, “Constraining minimum-norm inverse by phase synchronization and signal power of the scalp EEG channels,” IEEE Trans. Biomed Eng., vol. 56, no. 4, pp. 1228-1235, Apr. 2009.

[80] P. Celka, “Statistical analysis of the phase locking value,” IEEE Signal Process Lett., vol. 14, no. 9, Sep. 2007.

[81] A. Kraskov, and P. Grassberger, “MIC: mutual information based hierarchical clustering,” Information theory and statistical learning., CH. 5, pp. 101-123, Springer, 2009.

[82] M. Hutter, “Distribution of Mutual Information,” Advances in Neural Information Processing Systems., 2001

[83] D. P. Kingma, and J. L. Ba, “Adam: a method for stochastic optimization,” arXiv preprint arXiv:1412.6980, 2014.

[84] https://keras.io/

[85] C.-C. Chang, and C.-J. Lin, “LIBSVM : a library for support vector machines,” ACM Transactions on Intelligent Systems and Technology., vol.2, no. 3, 2011.

[86] C. Cortes, and V. Vapnik, “Support-vector networks,” Machine learning, vol. 20, no. 3, pp. 273–297, 1995.

[87] S. J. Hanrahan, J. Nedrud, B. S. Davidson, S. Farris, M. Giroux, A. Haug, M. H. Mahoor, A. K. Silverman, J. J. Zhang, A. O. Hebb, “Long-Term Task-and Dopamine-Dependent Dynamics of Subthalamic Local Field Potentials in Parkinson’s Disease,” Brain sciences., vol. 6, no. 4, 2016.

[88] P. Stoica and R. L. Moses, “Spectral Analysis of Signals,” Upper Saddle River., NJ:Prentice-Hall, 2005.

Appendix A

Publications

Patents

1. M. H. Mahoor, S. Niketeghad, A. O. Hebb, S. J. Hanrahan, J. Nedrud, and **H. M. Golshan**, "Motor Task Detection using Electrophysiological Signals," US Patent US10588534B2,. Mar. 2020.

Journal Papers

1. **H. M. Golshan**, Adam O. Hebb, and M. H. Mahoor, "LFP-net: A deep learning framework to recognize human behavioral activities using brain STN-LFP signals" Journal of Neuroscience Methods., vol. 335, pp. 108621, Jan. 2020.
2. **H. M. Golshan**, A. O. Hebb, S. J. Hanrahan, J. Nedrud, and M. H. Mahoor ," A hierarchical structure for human behavior classification using STN local field potentials," Journal of Neuroscience Methods., vol. 293, pp. 254-263, Jan. 2018.
3. H. Feng, **H. M. Golshan**, and M. H. Mahoor ,"A wavelet-based approach to emotion classification using EDA signals," Expert Systems with Applications., vol. 112, no. 1, pp. 77-86, Dec. 2018.

Conference Papers

1. **H. M. Golshan**, A. O. Hebb, J. Nedrud, and M. H. Mahoor ," Studying the effects of deep Brain stimulation and medication on the dynamics of STN-LFP signals for human behavior analysis," IEEE Int Conf on EMBC., July. 2018.
2. **H. M. Golshan**, A. O. Hebb, J. Nedrud, and M. H. Mahoor ,"Studying the effect of subthalamic stimulation and dopamine-dependent therapy on human behavior analysis using LFP signals," ASSFN Biennial Meeting., Jun. 2018.
3. **H. M. Golshan**, A. O. Hebb, S. J. Hanrahan, J. Nedrud, and M. H. Mahoor ,"An FFT-based synchronization approach to recognize human behaviors using STN-LFP signal," IEEE Int Conf on ICASSP, pp. 979-983, Mar. 2017.

4. **H. M. Golshan**, A. O. Hebb, S. J. Hanrahan, J. Nedrud, and M. H. Mahoor ,"A multiple kernel learning approach for human behavioral task classification using STN-LFP signal," IEEE Int Conf on EMBC., Aug. 2016.

5. A. O. Hebb, **H. M. Golshan**, S. J. Hanrahan, J. Nedrud, and M. H. Mahoor, "Behavior classification using multi-site LFP and ECoG signals," Conf on Society for Neuroscience, San Diego, Nov. 2016.